Cynomolgus Monkey as a Potential Model to Assess Drug Interactions Involving Hepatic Organic Anion Transporting Polypeptides (OATPs): *In Vitro*, *In Vivo* and *In Vitro*-to-*In Vivo* Extrapolation

Hong Shen, Zheng Yang, Gabe Mintier, Yong-Hae Han, Cliff Chen, Praveen Balimane, Mohammed Jemal, Weiping Zhao, Renjie Zhang, Sanjith Kallipatti, Sabariya Selvam, Sunil Sukrutharaj, Prasad Krishnamurthy, Punit Marathe, and A. David Rodrigues

Department of Pharmaceutical Candidate Optimization (H.S., Z.Y., Y.H., C.C., P.B., M.J., W.Z., P.M., A.D.R.), and Department of Genomic Technologies (G.M.), Bristol-Myers Squibb Research and Development, Princeton, NJ; Department of Molecular Biology (S.K., S.S., S.S., P.K.), Bristol-Myers Squibb Biocon R&D Center, Bangalore, India; Department of Bioanalytical Service (R.Z.), WuXi AppTec Co., Ltd, Shanghai, China

JPET Fast Forward. Published on January 7, 2013 as DOI: 10.1124/jpet.112.200691
This article has not been copyedited and formatted. The final version may differ from this version.

Running title: Use of Cynomolgus Monkey to Assess DDIs Involving OATPs

Corresponding author: Hong Shen, F1.3811, Route 206 & Province Line Road, Bristol-Myers Squibb Company, Princeton, NJ 08543-4000. Telephone: (609) 252-4509; Facsimile: (609) 252-6802; E-mail: hong.shen1@bms.com

Number of text pages: 28

Number of tables: 6

Number of figures: 5

Number of references: 44

Number of words:

Abstract: 246

Introduction: 753

Discussion: 1889

Abbreviations: AUC, area under the concentration-time curve; CCK-8, cholecystokinin octapeptide; C_{max}, maximum plasma concentration; cOATP, cynomolgus organic anion transporting polypeptide; CsA, Cyclosporin A; CYP3A4, cytochrome P450 3A4; DDI, drug-drug interaction; E3S, estrone-3-sulfate; E17βG, estradiol-17β-D-glucuronide; FRT, Flp recombination target; f_u, fraction of unbound drug; HBSS, Hank's balanced salt solution; HEK-293: human embryonic kidney 293 cells; hOATP, human organic anion transporting polypeptide; I_{ave}, average systemic concentration of inhibitor; $I_{in,max}$, estimated maximal inhibitor concentration at the inlet to the liver; I_{max}, maximum systemic plasma concentration of inhibitor;

JPET Fast Forward. Published on January 7, 2013 as DOI: 10.1124/jpet.112.200691
This article has not been copyedited and formatted. The final version may differ from this version.

ITC, International Transporter Consortium; IVIVE, *in vitro-in vivo* extrapolation; K_m, Michaelis-Menten constant that corresponds to the substrate concentration at which the uptake rate is half of V_{max}; OATP, organic anion transporting polypeptide; PCR, polymerase chain reaction; RIF: rifampin; RSV: rosuvastatin; V_{max}, maximum transport rate.

Recommended section: Metabolism, Transport and Pharmacogenomics

JPET Fast Forward. Published on January 7, 2013 as DOI: 10.1124/jpet.112.200691
This article has not been copyedited and formatted. The final version may differ from this version.

Abstract

Organic anion transporting polypeptides (OATP) 1B1, 1B3 and 2B1 can serve as the loci of drug-drug interactions (DDIs). Therefore, the cynomolgus monkey was evaluated as a potential model for studying OATP-mediated DDIs. Three cynomolgus monkey OATPs (cOATPs), with a high degree of amino acid sequence identity (91.9%, 93.5%, and 96.6% for OATP1B1, 1B3 and 2B1, respectively) to their human counterparts, were cloned, expressed and characterized. The cOATPs were stably transfected in human embryonic kidney cells and were functionally similar to the corresponding human OATPs (hOATPs), as evident from the similar uptake rate of typical substrates (estradiol-17β-D-glucuronide, cholecystokinin octapeptide and estrone-3-sulfate). Moreover, 6 known hOATP inhibitors exhibited similar IC_{50} values against cOATPs. To further evaluate the appropriateness of the cynomolgus monkey as a model, a known hOATP substrate (rosuvastatin, RSV)-inhibitor (rifampicin, RIF) pair was examined *in vitro* and the monkey-derived parameters (RSV K_m and RIF IC_{50}) were similar (within 3.5-fold) to those obtained with hOATPs and human primary hepatocytes. *In vivo*, the area under the plasma concentration-time curve of RSV (3 mg/kg, oral) 1 hour after a single RIF dose (15 mg/kg, oral) was increased 2.9-fold in cynomolgus monkeys, consistent with the value (3.0-fold) reported in humans. A number of *in vitro-in vivo* extrapolation approaches, considering the fraction of the pathways affected and free vs. total inhibitor concentrations, were explored also. It is concluded that the cynomolgus monkey has the potential to serve as a useful model for the assessment of OATP-mediated DDIs in a nonclinical setting.

JPET Fast Forward. Published on January 7, 2013 as DOI: 10.1124/jpet.112.200691
This article has not been copyedited and formatted. The final version may differ from this version.

Introduction

Drug-drug interactions (DDIs) have often been attributed to cytochrome P450 (CYP) enzymes because of their prominent role in the metabolic clearance of drugs (Vuppugalla et al., 2010). More recently, however, attention has turned to active transport processes in different organs and the close interplay between drug transport and metabolism at the cellular level. In particular, organic anion transporting polypeptides (OATPs) are known to mediate the active uptake of numerous drugs into hepatocytes and hence govern their overall clearance, pharmacokinetic profile and liver-to-plasma ratio (Giacomini et al., 2010; Fenner et al., 2012; Yoshida et al., 2012).

OATPs can also serve as the loci of important DDIs leading to changes in systemic and local drug concentrations, possibly resulting in altered efficacy and enhanced toxicity (Giacomini et al., 2010; Yoshida et al., 2012). For example, cyclosporin (CsA) increases the AUC (~15-fold) and C_{max} (~14-fold) of atorvastatin in healthy volunteers (Lemahieu et al., 2005). Such an interaction is attributed to inhibition of OATP-mediated atorvastatin uptake into the liver. Although the elimination of atorvastatin is dependent in part on cytochrome P450 3A4 (CYP3A4)-mediated metabolism, a less significant interaction (1.5- to 3.3-fold AUC increase) is observed with itraconazole, a potent CYP3A4 inhibitor (Mazzu et al., 2000; Kantola et al., 1998). Similarly, other DDIs involving atazanavir/ritonavir with rosuvastatin, gemfibrozil with repaglinide and CsA with pravastatin, among others, have also been ascribed to the inhibition of OATPs (Yoshida et al., 2012).

Recognizing the significance of DDIs involving OATPs, the US Food and Drug Administration and European Medicines Agency have included OATP1B1 and OATP1B3 as important transporters that should be considered when developing a new chemical entity. This is

reflected in a recently issued draft *DDI Guidance for Industry* (US Department of Health and Human Services; 2012) and *Guideline on the Investigation of Drug interactions* (European Medicines Agency; 2012). Likewise, OATP-mediated DDIs have also been the subject of a white paper published by The International Transporter Consortium (ITC) (Giancomini et al., 2010). In both publications, suggestions are made regarding the extrapolation of *in vitro* OATP results and the prediction of DDIs. However, over-predictions and a lack of consistency are apparent and it is evident that for any substrate one has to consider both active and passive uptake into hepatocytes, and take into account individual OATPs (Giancomini et al., 2010; Karlgren et al., 2012).

Given the difficulties of predicting DDIs based on *in vitro* data alone, a number of groups have turned to various animal models as a means of improving risk assessment prior to human dosing (Vuppugalla et al., 2010). In this regard, the cynomolgus monkey has been used increasingly as a model to support the characterization of drug disposition prior to detailed human studies and the conduct of mechanistic (DDI) studies (Akabane et al., 2010; Tang and Prueksaritanont, 2010). Moreover, when compared to other species, there is high sequence identity between numerous cynomolgus monkey and human drug-metabolizing enzymes and transporters (Iwasaki and Uno, 2009; Yasunaga et al., 2008; Tahara et al., 2005). For example, cOATP1B3 has been identified and cloned, shares 93.2% amino acid sequence identity with hOATP1B3 and is expressed exclusively in the liver (White et al., 2006). Furthermore, the substrate profile of cOATP1B3 is similar to that of hOATP1B3. A second monkey OATP (cOATP1B1) has been cloned and characterized also, and its substrate and inhibition profile is similar to that of hOATP1B1 (Maeda and Sugiyama, 2010). Information for additional cOATPs (e.g., cOATP2B1) is lacking.

As described herein, the cynomolgus monkey was further investigated as a preclinical model for studying OATP-mediated DDIs, with the possible strategies and considerations outlined in Fig. 1. This involved the cloning and expression of 3 different cOATPs in human embryonic kidney (HEK)-293 cells. Their activity was assessed and compared to three hOATPs using well-documented probe substrates (estradiol-17β-D-glucuronide, E17βG; cholecystokinin octapeptide, CCK-8; and estrone-3-sulfate, E3S). In addition, cOATP-mediated transport was studied in the presence of 6 known hOATP inhibitors and IC_{50}s were generated. The study was expanded to include a known OATP substrate (rosuvastatin, RSV)-inhibitor (rifampicin, RIF) pair, which involved an *in vitro-in vivo* extrapolation (IVIVE) exercise employing the IC_{50}s generated *in vitro* (cOATPs and suspensions of cynomolgus primary hepatocytes) and a single dose *in vivo* monkey DDI study. It is concluded that the cynomolgus monkey has the potential to serve as a model for the assessment of OATP-mediated DDIs. Once generated, the data can serve as a calibrator that links *in vitro* to *in vivo* and facilitates the selection of the most appropriate IVIVE approach when attempting to predict OATP inhibition prior to human dosing.

JPET Fast Forward. Published on January 7, 2013 as DOI: 10.1124/jpet.112.200691
This article has not been copyedited and formatted. The final version may differ from this version.

Material and Methods

Chemicals and Reagents. [^{3}H]E17βG (34.3 Ci/mmol), [^{3}H]CCK-8 (97.5 mCi/mmol), and [^{3}H]E3S ammonium salt (45.6 Ci/mmol) were purchased from PerkinElmer Life and Analytical Sciences (Waltham, MA). [^{3}H]RSV calcium (10 mCi/mmol) was obtained from American Radiolabeled Chemicals (St. Louis, MO). Radiochemical purity of all compounds was determined to be greater than 98.2% by HPLC. Cold E17βG, CCK-8, E3S, RIF, CsA, gemfibrozil, and verampamil were purchased from Sigma-Aldrich (St. Louis, MO). RSV calcium, ritonavir, and saquinavir were purchased from Toronto Research Chemicals Inc. (North York, Ontario). Cryopreserved human and cynomolgus primary hepatocytes for transport studies were purchased from Celsis *In Vitro* Technologies (Baltimore, MD). All other reagents were obtained from commercial sources.

Molecular Cloning of cOATP1B1, cOATP1B3, and cOATP2B1. Cynomolgus monkey transporters OATP1B1, OATP1B3, and OATP2B1 were cloned out of liver total RNA (BioChain, Newark, CA). Maxima reverse transcriptase (Fermentas, Glen Burnie, MD) was used for cDNA synthesis following the manufacturer's recommended protocol. cDNA synthesis was primed with Oligo(dT)$_{18}$. The following polymerase chain reaction (PCR) primers were designed against highly conserved regions outside the coding sequence based on nucleotide sequence alignments from species orthologs. OATP1B1: 5'TGTTGCAGTTGCTGTAGGATTC 3' (forward primer), 5' TCTTACTGAATCAATGCAATGCTG 3' (reverse primer); OATP1B3: 5'CACATGGTATCTGTAGTTTAATCATG 5' (forward primer), 5'AAATAACATCTTAATGAATCAATACAATGTTA 3' (reverse primer); OATP2B1: 5'TCACTGCACTGCAGCAGTCATG 3' (forward primer), 5'GGGGCCCCAGGACGGCTCA 3' (reverse primer). All primers were obtained from Sigma Aldrich (St. Louis, MO). PCR

JPET Fast Forward. Published on January 7, 2013 as DOI: 10.1124/jpet.112.200691
This article has not been copyedited and formatted. The final version may differ from this version.

products were cloned into pJet1.2 (Fermentas) and several clones for each cDNA were sequenced. Sequences were deposited to GenBank: OATP1B1 (ACC# JX866725), OATP1B3 (ACC# JX866726), and OATP2B1 (ACC# JX866727). The coding sequence of each cDNA was subcloned into the Gateway entry vector pDONR221 (Invitrogen, Carlsbad, CA) using standard methods. The Gateway entry clones were recombined into a Gateway adapted version of the expression vector pcDNA5/FRT/TO (Invitrogen, Carlsbad, CA) using LR clonase II (LifeTechnologies, Carlsbad, CA) according to the manufacturer's protocol. Expression constructs were analyzed by agarose gel electrophoresis and the sequence was confirmed.

Generation of Stable cOATP1B1-, cOATP1B3-, and cOATP2B1-Transfected Cell Lines and Cell Cultivations. Stable transfection of HEK-293 cells with cOATPs, using Lipofectamine 2000 and the Flp-In expression system, was carried out as described previously (Shen et al., 2011). In brief, the recombinant pcDNA5/ Flp recombination target (FRT) construct containing either cOATP1B1, or cOATP1B3, or cOATP2B1 was co-transfected with pOG44, a Flp recombinase expression plasmid, into the Flp-In HEK-293 cell line using Lipofectamine 2000 (Invitrogen; Carlsbad, CA). The cells stably expressing the transporters were then selected with HEK-293 cell medium (Dulbeccos's modified eagle's medium supplemented with 10% fetal bovine serum, 0.1 mM nonessential amino acids, 2 mM L-glutamate) supplemented with selecting antibiotic hygromycin B (100 μg/ml). Single hygromycin-resistant colony cells were sorted into 24-well plates containing HEK-293-conditioned medium. After expansion, clones were screened for expression of functional transporter activity on the basis of increased transport of probe substrate and PCR analysis. For continued culturing, the stable clones were cultivated in hygromycin B supplemented HEK-293 medium.

JPET Fast Forward. Published on January 7, 2013 as DOI: 10.1124/jpet.112.200691
This article has not been copyedited and formatted. The final version may differ from this version.

All cells (cOATP- and hOATP-transfected HEK-293 cells and mock cells) were cultured at 37°C in an atmosphere of 95% air and 5% CO_2 and sub-cultured once a week. Passage numbers 5 to 30 were used throughout the study to keep the transporter expression level and functional activity consistent (unpublished in-house data). All cell culture media and reagents were obtained from Invitrogen (Carlsbad, CA) or Mediatech, Inc (Manassas, VA). Two to three days prior to performing the transport experiments, cells were seeded in 24-well poly-D-lysine coated plates (BD Biosciences; San Jose, CA) at a density of 500,000 cells per well.

HEK-293 cells containing individual expressed hOATP1B1, hOATP1B3, and hOATP2B1 were prepared as described previously (Han et al., 2010).

Uptake and Inhibition Studies Using Transporter-Expressing HEK-293 Cells. Transport experiments were performed based on the protocol described previously with minor modifications (Han et al., 2010). Briefly, cells were rinsed twice with 1.5 ml of pre-warmed Hanks' balanced salt solution (HBSS), followed by incubation at 37 °C with pre-warmed standard buffer (HBSS with 10 mM HEPES, pH 7.4) containing radiolabeled compounds ([^{3}H]E17βG, [^{3}H]CCK-8, [^{3}H]E3S, or [^{3}H]RSV). Subsequently, the incubations were stopped at the designated time by removing the buffer and rinsing the cells three times with 1 ml of ice-cold HBSS solution. [^{3}H]E17βG, [^{3}H]CCK-8, and [^{3}H]E3S uptake was assessed over a period of 1.5 minutes to ensure linearity with time (unpublished in-house data). Based on the linear conditions established (Supplementary Fig. 3), [^{3}H]RSV uptake into HEK-293 cells expressing cOATP1B1, hOATP1B1, cOATP2B1, and hOATP2B1 was determined over 1.5 min. Assessment of [^{3}H]RSV uptake into HEK-293 cells expressing cOATP1B3 and hOATP1B3 involved a 5 min incubation. The cells were lysed with 0.3 ml of 0.1% Triton X-100, and the radioactivity was determined by liquid scintillation counting. Accumulation was normalized to

JPET Fast Forward. Published on January 7, 2013 as DOI: 10.1124/jpet.112.200691
This article has not been copyedited and formatted. The final version may differ from this version.

the protein content of the HEK-293 cells in each well measured using the BCA protein assay kit (Pierce Chemical, Rockfold, IL).

To characterize species-dependent inhibition profiles, cells grown in 24-well plates were incubated with a test solution containing a probe substrate (1 μM E17βG, 0.1 μM CCK-8, or 1 μM E3S) to enable inhibition curves to be derived for the 6 selected OATP inhibitors (RIF, CsA, ritonavir, gemfibrozil, verapamil and saquinavir). For the assessment of RSV uptake kinetics, a constant amount of radiolabel with varying amounts of unlabeled substrate was used. IC_{50} values for RIF with HEK-293 cells expressing each cOATP or hOATP were generated at a low concentration of RSV (0.1 μM). In all cases, uptake values in transfected HEK-293 cells were corrected by subtracting the passive uptake in mock cells.

Uptake and Inhibition Studies Using Cynomolgus Monkey and Human Primary Hepatocytes. Transporter-qualified cryopreserved cynomolgus monkey and human hepatocytes were obtained commercially (Celsis IVT, Baltimore, MD) and were thawed according to the supplier's standard method: hepatocytes were thawed at 37°C then placed in ice, after which the cells were poured into 37°C InVitroGRO-HT thawing medium at a ratio of 5 million cells/50 ml in a conical tube. The cells were then centrifuged at 50x *g* for 3 min and resuspended to 2×10^6 cells/ml in Krebs Henseleit buffer (pH 7.4). Hepatocyte viability was determined by trypan blue exclusion and only those hepatocyte preparations with viabilities greater than 80% were used. One lot of cryopreserved cynomolgus monkey hepatocytes (pool of four male animals; Lot VCE) and 3 lots of cryopreserved human primary hepatocytes (Lots OJE, GST, LIO; all male organ donors) were chosen based on relatively high transport activity. Cryopreserved human hepatocytes from the three donors were pooled together after thawing for the uptake study.

JPET Fast Forward. Published on January 7, 2013 as DOI: 10.1124/jpet.112.200691
This article has not been copyedited and formatted. The final version may differ from this version.

Cell suspensions were prewarmed in an incubator at 37°C for 3 min before the start of the uptake study. The uptake studies were then initiated by the addition of an equal volume of buffer containing [^{3}H]RSV (0.1 μM) with or without RIF (final cell concentration: 1×10^6 cells/ml). Aliquots were taken and placed in a narrow tube containing silicone-mineral oil (density, 1.015; Sigma-Aldrich, St. Louis, MO) on the top of 3 M potassium hydroxide solution, followed by centrifugation through the silicone-mineral oil layer at the designated time points (20 and 90s) to separate cells from media. The subsequent cell pellet was then lysed in potassium hydroxide solution overnight at room temperature. The radioactivity in both cells and media was determined by liquid scintillation counting.

Pharmacokinetic DDI Study Employing Cynomolgus Monkeys. The *in vivo* studies were carried out by WuXi AppTec (Suzhou, China) using 3 male cynomolgus monkeys (between 4 and 6 kg of body weight) in a crossover fashion, with a 3-week washout period.

The same 3 animals were used in all studies described below. In the first period, each monkey received RSV (3 mg/kg) dissolved in water by oral gavage followed by a sterile water rinse, and blood samples were collected at 0.25, 0.5, 0.75, 1, 2, 3, 5, 7, and 24 h postdose in K_2-EDTA-containing tubes. After the centrifugation of blood samples for 3 min at 13,000 rpm, the resultant plasma was stored at −20°C until analysis. In the subsequent period, a RSV water solution (3 mg/kg) was administered orally to each monkey one hour after RIF (15 mg/kg, PO; dissolved in polyethylene glycol 400). Blood was withdrawn to determine plasma levels of RSV and RIF (0.25, 0.5, 0.75, 1, 2, 3, 5, 7, and 24 h postdose of RSV). Throughout the study, monkeys were fasted before each dose of RSV or RIF.

LC-MS/MS Analysis of RSV. Stock solutions (1 mg/ml) of RSV and rosuvastain-5S-lactone, a metabolite of RSV, were prepared in acetonitrile/1 mM ammonium acetate pH 4.0 buffer (80:20

JPET Fast Forward. Published on January 7, 2013 as DOI: 10.1124/jpet.112.200691
This article has not been copyedited and formatted. The final version may differ from this version.

v/v). A stock solution (0.200 mg/ml) of atorvastatin (internal standard) was prepared in 50% acetonitrile. The following RSV calibration standards were prepared in monkey plasma: 0.300, 0.600, 3.00, 30.0, 150, 300, 600 and 750 ng/ml of plasma. Quality control (QC) samples were also prepared in monkey plasma: 0.900, 15.0, 270, 570 and 1500 ng/ml of plasma. The 1500 ng/ml dilution QC was diluted 1 to 20 with blank plasma before analysis. Additionally, a 20 ng/ml lactone-only QC, which contains only rosuvastain-5S-lactone, was prepared.

Plasma sample extraction for RSV was conducted in a 96-well plate using protein precipitation with acetonitrile containing 0.5% formic acid. In brief, 50 µl of calibration standards, QC samples and study plasma samples were mixed first with 50 µl of chilled (ice/water bath) 0.1 M ammonium acetate buffer (pH 4.5) and then with 20 µl of chilled 100 ng/ml atorvastatin solution in acetonitrile/1 mM ammonium acetate pH 4.0 buffer (80:20 v/v). Following the addition of 400 µl chilled 0.5% formic acid in acetonitrile, vortex-mixing and centrifugation at 4°C, an aliquot of 200 µl of each sample was transferred to a new 96-well plate and then 200 µl of chilled 1 mM ammonium acetate buffer (pH 4.0) was added. A 10-µl aliquot was injected for analysis by LC-MS/MS.

The HPLC system consisted of an Agilent 1200 pump, Agilent 1200 column oven (Agilent Technologies, Santa Clara, CA) and a CTC PAL autosampler (CTC Analytics AG, Zwingen, Switzerland) maintained at 4^{o}C during analysis. The analytical column used was a Shiseido CAPCELLPAK MG C18 (2.0 x 50 mm, 5.0 µm; Shiseido Co., Japan) and was maintained at 40^{o}C. The mobile phase consisted of pH 4.0, 1 mM ammonium acetate buffer (eluent A) and 100% acetonitrile (eluent B). The following gradient elution was used: start and maintain at 30% B from 0 to 0.5 min; ramp from 30% to 70% B from 0.5 to 1.5 min; hold at 70% B from 1.5 to 2.5 min; ramp to 30% B from 2.5 to 2.51 min; hold at 30% B until 3.7 min before the next

JPET Fast Forward. Published on January 7, 2013 as DOI: 10.1124/jpet.112.200691
This article has not been copyedited and formatted. The final version may differ from this version.

injection. The flow rate was 0.4 ml/min. The retention times of RSV, atorvastatin and rosuvastain-5S-lactone were 2.05, 2.40 and 2.30 min, respectively.

The HPLC was interfaced to a Sciex API 5000 mass spectrometer (MDS SCIEX, Concord, Ontario, Canada). The following positive electrospray (ESI) source/gas conditions were used: curtain gas at 25; ion spray voltage at 5500; temperature at 550^{o}C; ion source gas 1 at 40; ion source gas 2 at 50. The compound-dependent parameters used for RSV, atorvastatin and rosuvastain-5S-lactone were, respectively, as follows: declustering potential of 80, 80, 80; collision energy of 48, 30, 48; collision cell exit potential of 14, 14, 14. The multiple reaction monitoring (MRM) transitions used were as follows: *m/z* 482.2 → *m/z* 258.1 for RSV, *m/z* 559.3 → *m/z* 440.2 for atorvastatin, and *m/z* 464.2 → *m/z* 270.1 for rosuvastain-5S-lactone.

In order to avoid the conversion of rosuvastatin-5S-lactone metabolite to RSV, the thawing of plasma samples stored frozen at ≤ -70^{o}C was conducted at 4°C (ice/water) and the aliquots for analysis were mixed with a pH 4.5 buffer since moderately lower pH minimizes conversion of the lactone metabolite. For the same reason, the acetonitrile used for protein precipitation and the reconstitution solution were both acidified. In order to avoid assay bias due to potential conversion of the metabolite in the mass spectrometer, the chromatographic conditions were optimized to achieve the separation of the lactone metabolite from rosuvastatin. In addition, a special quality control (QC) sample that contained only rosuvastain-5S-lactone (lactone-only QC) was included in every sample analysis run to gauge any conversion of the metabolite to RSV. The performance of this QC showed that the conversion was minimal (less than 5%) and thus the metabolite in the study samples does not contribute to the measured RSV concentrations

LC-MS/MS Analysis of RIF. Stock solutions (1 mg/ml) of RIF and tri-deuterated RIF (D_3-RIF, internal standard) were prepared in 0.1% ascorbic acid in 75% methanol (methanol/water:

JPET Fast Forward. Published on January 7, 2013 as DOI: 10.1124/jpet.112.200691
This article has not been copyedited and formatted. The final version may differ from this version.

75:25 v/v). The concentrations of RIF calibration standards in monkey plasma containing 0.1% ascorbic acid were 20.0, 50.0, 250, 1000, 2500, 5000 and 10000 ng/ml of plasma. The QC samples were 60.0, 500 and 7500 ng/ml.

Plasma sample extraction for RIF was conducted in 96-well plate using protein precipitation with acetonitrile containing 0.2% butylated hydroxytoluene. In brief, 50 µl of calibration standards, QC samples and study plasma samples were mixed with 50 µl of 3000 ng/ml internal standard (D_3-RIF) in 0.1% ascorbic acid in 75% methanol. Following the addition of 300 µl 0.2% butylated hydroxytoluene in acetonitrile, vortex-mixing and centrifugation at 4°C, an aliquot of 200 µl of each sample was transferred to a new 96-well plate and then 200 µl of 20% acetonitrile was added. After transferring 100 µl of each sample to a new plate and adding 300 µl of 20% acetonitrile, a 10 µl aliquot was injected for analysis by LC-MS/MS.

The HPLC system consisted of Shimadzu 20 series pump and CTC PAL autosampler maintained at 4^{o}C. The analytical column used was an Agilent Eclipse C18 (2.1 x 50 mm, 5.0 µm; Agilent Technologies, Santa Clara, CA) and was maintained at 40^{o}C. The mobile phase consisted of 0.2% acetic acid in water (eluent A) and 100% acetonitrile (eluent B). The following gradient elution was used: start and maintain at 30% B from 0 to 0.3 min; ramp from 30% to 100% B from 0.3 to 1.3 min; hold at 100% B from 1.3 to 2.5 min; ramp to 30% B from 2.5 to 2.6 min; hold at 30% B until 3.2 min before the next injection. The flow rate was 0.4 ml/min. Retention times of RIF and D_3-RIF were 1.25 and 1.25 min, respectively.

The HPLC was interfaced to a Sciex API 4000 mass spectrometer (MDS Sciex, Concord, ON, Canada). The following positive ESI source/gas conditions were used: curtain gas at 25; ion spray voltage at 5000; temperature at 500^{o}C; ion source gas 1 at 55; ion source gas 2 at 50. The compound-dependent parameters used for RIF and D_3-RIF were, respectively, as follows:

JPET Fast Forward. Published on January 7, 2013 as DOI: 10.1124/jpet.112.200691
This article has not been copyedited and formatted. The final version may differ from this version.

declustering potential of 60, 81; collision energy of 25, 36; collision cell exit potential of 14, 10. The MRM transitions used were as follows: *m/z* 823.4 → *m/*z 791.7 for RIF and *m/z* 826.6 → *m/*z 402.3 for D_3-RIF.

IVIVE-Based Prediction of DDI Between RSV and RIF Involving the Inhibition of OATPs. Three equation-based approaches were used in the IVIVE exercise for predicting the OATP-mediated DDI between RSV and RIF.

$$\frac{AUC_i}{AUC_c} = 1 + \frac{I}{K_{i,OATPs}} \quad \text{Eq. 1}$$

$$\frac{AUC_i}{AUC_c} = \frac{1}{\frac{f_{OATPs}}{1 + I/K_{i,OATPs}} + (1 - f_{OATPs})} \quad \text{Eq. 2}$$

$$\frac{AUC_i}{AUC_c} = \frac{1}{\frac{f_{OATP1B1}}{1 + I/K_{i,OATP1B1}} + \frac{f_{OATP1B3}}{1 + I/K_{i,OATP1B3}} + (1 - f_{OATP1B1} - f_{OATP1B3})} \quad \text{Eq. 3}$$

where AUC_i and AUC_c are the AUC in the presence and absence of an inhibitor, respectively; f_{OATPs}, $f_{OATP1B1}$, and $f_{OATP1B3}$ are the fraction of total clearance that undergoes clearance mediated by OATPs, OATP1B1, and OATP1B3, respectively; $K_{i,OATPs}$, $K_{i,OATP1B1}$, $K_{i,OATP1B3}$ are the inhibitory constant against the clearance mediated by OATPs, OATP1B1, and OATP1B3, respectively. Eq. 1 was described previously for transporter-based DDIs by Giancomini et al. (2010) and is currently recommended in the Food and Drug Administration draft DDI Guidance for Industry (US Department of Health and Human Services, 2012). The equation represents the most conservative case, assuming competitive inhibition by a perpetrator drug and that the rate-limiting step in drug clearance from plasma is entirely mediated by uptake transporters such as OATPs. Eq. 2 takes into consideration that about 28% of the total RSV clearance in humans is renal (Martin et al., 2003b). Assuming that the renal clearance of RSV is not affected by RIF,

JPET Fast Forward. Published on January 7, 2013 as DOI: 10.1124/jpet.112.200691
This article has not been copyedited and formatted. The final version may differ from this version.

the fraction (f_{OATP}) of the total body clearance affected by RIF due to the inhibition of OATPs was estimated to be 0.72. The same f_{OATP} was assumed for both humans and cynomolgus monkeys. Furthermore, the OATP-mediated clearance can be fractionated into OATP1B1- and OATP1B3-mediated uptake processes due to the different contribution of OATPs to the hepatic uptake of RSV, as well as the differential inhibitory effects of RIF. Using the relative activity factor method (Kitamura et al., 2008), the average contributions of OATP1B1 and OATP1B3 to the hepatic uptake of RSV in human hepatocytes (N = 3 lots) were estimated to be 77.0 and 23.0%, respectively. Accordingly, the fraction ($f_{OATP1B1}$ and $f_{OATP1B3}$) of OATP1B1- and OATP1B3-mediated uptake clearance relative to the total body clearance of RSV were calculated to be 0.554 (0.72*0.77) and 0.166 (0.72*0.23), respectively. As described by Rodrigues et al. (2001) for individual P450 enzymes, Eq. 3 was used to account for OATP1B1- and OATP1B3-mediated individual uptake processes. In the IVIVE, the $f_{OATP1B1}$ and $f_{OATP1B3}$ were assumed to be the same between humans and cynomolgus monkeys.

In the present study, the substrate concentration used for the inhibition studies was well below the K_m. Hence, assuming competitive inhibition, the concentration (IC_{50}) that corresponds to the 50% of the maximum inhibition can be substituted for the K_i in Eqs. 1-3. For Eqs. 1-2, the IC_{50} values determined with human and cynomolgus monkey hepatocytes were used for the IVIVE. For Eq. 3, the IC_{50} obtained from the HEK-293 cells expressing individual OATPs was used.

Selecting the appropriate inhibitor concentration to use (Eqs. 1-3) is also critical to a successful IVIVE. In the present study, therefore, I_{max}, I_{ave}, and $I_{in,max}$ were all used. The $I_{in,max}$ was calculated using the following equation.

$$I_{in,max} = I_{max} + \frac{k_a \text{ x } F_a \text{ x } F_g \text{ x } Dose}{Q_h} \qquad \text{Eq. 4}$$

JPET Fast Forward. Published on January 7, 2013 as DOI: 10.1124/jpet.112.200691
This article has not been copyedited and formatted. The final version may differ from this version.

where k_a is the absorption rate constant of the inhibitor; $F_a x F_g$ is the fraction of the inhibitor dose absorbed into the portal vein, and Q_h is the hepatic blood flow (1,500 and 220 ml per min in humans and monkeys, respectively). The k_a and $F_a x F_g$ in humans, based on the literature values (Acocella et al., 1978; Mehta et al., 1985), were calculated to be 0.02 min^{-1} and unity, respectively. These parameters were assumed to be same between humans and cynomolgus monkeys. In addition, the use of free and total inhibitor concentrations was explored also. In this case, the plasma free fraction of RIF in humans and cynomolgus monkeys was 20% (Acocella et al., 1978; Sanofi-Aventis, 2005) and 19% (in-house data), respectively.

Data Analysis. *Kinetic Analysis.* The initial hepatic uptake velocity at each concentration of RSV (v) was calculated from the slope of cellular uptake versus time, and the kinetic parameter describing the hepatic uptake of RSV was obtained using the following equation:

$$v = \frac{V_{max} \times C}{K_m + C} + P_{diff} \times C \qquad \text{Eq. 5}$$

where P_{diff} is the nonsaturable clearance via passive diffusion; V_{max} represents the maximum rate of the saturable uptake; K_m is the Michaelis-Menten constant that corresponds to the substrate concentration at which the uptake rate is half of V_{max}. These parameters were estimated by fitting of the v-c data using nonlinear regression in WinNonlin (Pharsight Inc.; Mountain View, CA). The intrinsic active uptake was calculated by dividing the V_{max} by the K_m, whereas the total uptake clearance included both the active and passive components. Based on these parameters, the relative importance of the active hepatic uptake in comparison with the passive diffusion process can be estimated at therapeutically relevant concentrations.

JPET Fast Forward. Published on January 7, 2013 as DOI: 10.1124/jpet.112.200691
This article has not been copyedited and formatted. The final version may differ from this version.

The uptake of RSV into cynomolgus monkey and human OATP-expressing HEK-293 cells was evaluated after subtracting the uptake in mock-transfected cells from the total uptake in cOATP- and hOATP-expressing HEK-293 cells, and the kinetics was characterized using Eq. 6:

$$v = \frac{V_{\max} \text{ x } C}{K_m + C} \qquad \text{Eq. 6}$$

IC_{50} Determination. The IC_{50} was determined by fitting the data to the following equation using WinNonlin (Pharsight Inc.; Mountain View, CA).

$$v = V_{\max} \text{ x} \left(1 - \frac{I^{\gamma}}{I^{\gamma} + IC_{50}^{\gamma}} \right) \qquad \text{Eq. 7}$$

where γ is the Hill factor that describes the steepness of the curve, *I* is the inhibitor concentration and v is the rate of uptake measured at the given inhibitor concentration.

Pharmacokinetic and Statistical Analysis. Data are expressed in mean ± SD. The noncompartmental analyses of RSV and RIF plasma concentration-time data were performed using Kinetica (Thermo Fisher Scientific, Waltham, MA). Student's t-test (GraphPad Software, Inc., San Diego, CA) was used to compare the rates of substrate uptake between OATP-transfected and mock cells. A p-value of less than 0.05 was considered to be statistically significant.

JPET Fast Forward. Published on January 7, 2013 as DOI: 10.1124/jpet.112.200691
This article has not been copyedited and formatted. The final version may differ from this version.

Results

Cloning and Sequencing of cOATP1B1, cOATP1B3, and cOATP2B1 cDNAs. PCR primers based on the coding regions of human and rhesus OATP sequences were used to amplify full-length fragments from cynomolgus monkey liver cDNA. The complete cDNA sequences of cOATP1B1 and cOATP2B1, in this study, are reported for the first time (Supplementary Fig. 1A and 1C). The consensus cOATP1B3 sequence showed three amino acid residue differences (Lys291, Asn313 and Met577) when compared with the previously cloned cynomolgus monkey OATP1B3 sequence (GenBank accession number AY787036). The latter has Arg, Asp and Val at the same positions, respectively (White et al., 2006). However, amino acids at the specific positions in our sequence and the ones predicted from the cynomolgus monkey genomic sequence published recently did match (data not shown) (Ebeling et al., 2011). The alignment of sequences confirmed that the amino acids at those three positions among hOATP1B3, rhesus monkey OATP1B3 (rOATP1B3) and cOATP1B3 cloned by us are identical (Supplementary Fig. 1B).

Comparison of the cOATP sequences to the GenBank database of human and rhesus OATP cDNAs revealed that cOATP proteins are highly homologous to the human orthologs, and the corresponding cOATP1B1, cOATP1B3, and cOATP2B1 amino acid sequences are 91.9%, 93.5% and 96.6% identical to hOATP1B1, hOATP1B3, and hOATP2B1, respectively (Table 1; Supplementary Fig. 1).

Functional Characterization of cOATP1B1, cOATP1B3, and cOATP2B1 Expressed in HEK-293 Cells. cOATP1B1-, cOATP1B3-, and cOATP2B1-expressing HEK-293 cells were generated using FRT integrating plasmids introduced by transfection and selected with hygromycin. Hygromycin-resistant cells were then cloned, expanded and characterized. Real-

JPET Fast Forward. Published on January 7, 2013 as DOI: 10.1124/jpet.112.200691
This article has not been copyedited and formatted. The final version may differ from this version.

time PCR analysis showed that the cynomolgus OATP mRNAs were specifically over-expressed in the cOATP-transfected cells relative to mock-transfected cells (data not shown).

Transport Activity. HEK-293 cells stably expressing the individual monkey and human OATPs were functionally characterized by measuring the uptake rate of 3 model substrates under the same assay conditions (N = 3 for each experiment). As shown in Fig. 2A, E17βG uptake was significantly higher in hOATP1B1-expressing cells (45 ± 4.2 pmol/mg/1.5 min) vs. mock-transfected cells (1.3 ± 0.3 pmol/mg/1.5 min), although a significant difference ($p < 0.05$) in the uptake rate of E17βG into hOATP1B3- and hOATP2B1-expressing cells was observed also. For the cOATPs, the rate of E17βG uptake into cOATP1B1-, cOATP1B3-, and cOATP2B1-expressing cells was 24 ± 2.8, 14 ± 1.4, and 2.5 ± 0.6 pmol/mg/1.5 min, respectively, significantly higher than that of mock-transfected cells ($p < 0.05$). With CCK-8 as substrate, the uptake rate into cOATP1B3- and hOATP1B3-expressing cells (5.5 ± 0.7 and 3.5 ± 0.3 pmol/mg/1.5 min, respectively) was significantly higher than that observed with mock-transfected cells (0.3 ±0.1 pmol/mg/1.5 min, Fig. 2B). A statistically significant difference from the mock control was also observed with cOATP1B1 (0.7 ± 0.1 pmol/mg/1.5 min, $p < 0.05$) but not the other OATPs. For the third substrate, E3S, the highest rate of uptake (versus mock cells) was observed with cOATP2B1- and hOATP2B1-expressing cells (229 ± 25 and 351 ± 71 pmol/mg/1.5 min, respectively; vs. 3.3 ± 0.3 pmol/mg/1.5 min). Although statistically significant, the difference in the uptake rate of E3S (vs mock cells) was reduced for the other cOATPs and hOATPs (Fig. 2C). Under the assay conditions described herein, therefore, the substrate profile of cOATPs was more or less similar to that of hOATPs. Also, the present hOATP uptake results were in agreement with the previous data (Han et al., 2010).

JPET Fast Forward. Published on January 7, 2013 as DOI: 10.1124/jpet.112.200691
This article has not been copyedited and formatted. The final version may differ from this version.

Inhibition of Transport Activity. Once the assays were in place it was possible to assess the inhibition of OATP-mediated transport into HEK-293 cells. Towards this end, 6 known hOATP inhibitors were chosen that would render a wide range of IC_{50} values (Table 2). All 6 compounds inhibited both cOATPs and hOATPs almost equally, and their IC_{50}s were in good agreement for each OATP form (less than 3-fold difference) (Fig. 3). Of the 6 compounds tested, RIF was the most potent inhibitor of both cOATP1B1 and hOATP1B1 (IC_{50} of 0.20 ± 0.08 and 0.55 ± 0.07 μM, respectively). RIF was also the most potent inhibitor of hOATP1B3 (IC_{50} of 0.46 ± 0.13 μM). But for cOATP1B3 RIF was less potent than CsA. Interestingly, all of the compounds consistently showed less inhibition of OATP2B1 (versus OATP1B1 and OATP1B3) (Table 2).

***In Vitro* Uptake of RSV by Cynomolgus Monkey and Human Cryopreserved Hepatocytes and Individual OATP-Expressing HEK-293 Cells.** RSV was selected as a probe substrate to support the IVIVE exercise, because its liver uptake is mainly dependent on OATPs and it undergoes relatively little metabolism (Kitamura et al., 2008; Martin et al., 2003c).

Uptake of RSV into Hepatocytes. RSV hepatic uptake was assessed with pooled cynomolgus and human cryopreserved hepatocytes. As expected, a time- and temperature-dependent increase in RSV hepatic uptake was observed, and the uptake difference between two time points (20 sec versus 90 sec) was used to calculate the initial uptake rate over a wide RSV concentration range (0.06-100 μM). The use of such a wide RSV concentration range afforded the robust assessment of active uptake and allowed sufficient data points to determine kinetic parameters (Supplementary Fig 2). The model for 1 saturable component plus 1 passive diffusion process (Eq. 5) described the monkey hepatocyte data well, resulting in a single uptake K_m of 6.7 ± 0.8 μM and a V_{max} of 172.3 ± 9.5 pmol/min/10^6 cells (P_{diff} = 0.7 ± 0.1 μl/min/10^6 cells). Similar

JPET Fast Forward. Published on January 7, 2013 as DOI: 10.1124/jpet.112.200691
This article has not been copyedited and formatted. The final version may differ from this version.

parameter estimates were obtained from human hepatocytes (Table 3). The V_{max} of RSV in monkeys and intrinsic active uptake clearance (V_{max}/K_m) were about 2-fold higher than those of humans, suggesting better transporter activity and/or viability with monkey hepatocytes versus human cells. In addition, when the active uptake data were plotted using the Eadie-Hofstee equation, only a straight line was observed, demonstrating that either a single transporter or multiple transporters with indistinguishable K_m values are involved in the hepatic uptake of RSV (Supplementary Fig. 2E and 2F).

The active uptake of RSV, expressed as a percentage of total hepatic uptake, was 97% and 96% in monkeys and humans, respectively, suggesting a dominant role of active uptake to the overall RSV hepatic uptake process (Table 3; Supplementary Fig. 2). In agreement, a saturable uptake mechanism (> 88% of uptake) has been proposed for RSV in rats (Yabe et al., 2011). Therapeutically, the maximum plasma concentration of RSV has been reported to be 12.1 and 60.1 nM after single oral doses of 20 and 80 mg, respectively (Martin et al., 2003a, 2003b and 2003c). These values are well below the apparent K_m describing active uptake in human hepatocytes *in vitro*. Taken together, the present data suggest that, at therapeutically relevant concentrations, active processes play a major role in the uptake of RSV into hepatocytes.

Studies with HEK-293 Cells. To identify which transporters are involved in the hepatic active uptake of RSV in monkeys and humans, studies were performed in HEK-293 cells that stably expressed individual OATP transporters. The studies revealed that RSV was a substrate of all three OATPs in both species. As the RSV concentration increase from 60 nM to 100 μM, the uptake into mock cells increased linearly, whereas the uptake into transporter-expressing cells was nonlinear (data not shown). After subtracting uptake into mock cells from each transporter-expressing cell line, the transport kinetic profile was analyzed with the model containing a single

JPET Fast Forward. Published on January 7, 2013 as DOI: 10.1124/jpet.112.200691
This article has not been copyedited and formatted. The final version may differ from this version.

saturable component (Eq. 6). The saturable uptake of RSV into cOATP1B1-, cOATP1B3- and cOATP2B1-HEK293 cells was characterized as a single K_m (14.4 ± 3.0, 14.5 ± 2.0 and 9.6 ± 0.8 μM, respectively, Table 3). Similar K_m values were obtained with hOATP1B1, hOATP1B3, and hOATP2B1 (Table 3). The fact that these K_m values were similar is consistent with a single K_m derived from cynomolgus monkey and human hepatocytes.

RIF as an Inhibitor of RSV Uptake into Hepatocytes and OATP-Expressing HEK-293 Cells. The inhibitory effects of RIF on the uptake of [^{3}H]RSV into cynomolgus monkey and human hepatocytes were examined in the present study. RIF inhibited the uptake of RSV in a concentration-dependent manner and rendered IC_{50} values of 0.28 ± 0.16 μM (monkey) and 0.90 ± 0.45 μM (human). Similar IC_{50}s were obtained for the inhibition of RSV uptake into HEK-293 cells expressing cynomolgus monkey and human OATP1B1 and OATP1B3 (Table 4). On the other hand, both cOATP2B1- and hOATP2B1-mediated uptake of RSV into HEK-293 cells was weakly inhibited by RIF (IC_{50} of 81.6 ± 15.2 and 89.8 ± 5.4 μM, respectively). These results suggest that RIF likely affects OATP1B1 and 1B3, but not 2B1, at its therapeutically relevant concentrations in both cynomolgus monkeys and humans.

Effects of RIF on RSV Pharmacokinetics in Cynomolgus Monkeys. To assess the inhibitory effect of RIF on the OATP-mediated RSV uptake *in vivo*, a single-dose DDI study was conducted with male cynomolgus monkeys. The plasma concentration-time profile of RSV after administration of RSV alone or in combination with RIF is presented in Fig. 4A. The administration of RIF (15 mg/kg), 1 h before the dosing of RSV, resulted in a significant increase in RSV systemic exposure (i.e., $AUC_{0\text{-inf}}$ of 439 ± 110 versus 176 ± 109 nM•hr, respectively, Table 5 and Supplementary Fig. 4). Treatment with RIF also caused a substantial increase in the C_{max} (from 16.4 ± 11.7 to 113.2 ± 29.0 nM). While the t_{max} of RSV was decreased (5-fold) in the

JPET Fast Forward. Published on January 7, 2013 as DOI: 10.1124/jpet.112.200691
This article has not been copyedited and formatted. The final version may differ from this version.

presence of RIF (from 5.0 and 1.0 hr), the $t_{1/2}$ of RSV was similar between the two treatments (i.e., 6.1 vs. 5.8 hr).

The pharmacokinetics of RIF in monkeys was also evaluated. At an oral dose of 15 mg/kg, RIF plasma levels reached a peak of 9.2 μM, with a t_{max} of 3.3 hr (Fig. 4B). The AUC over a 25-hr period was 67.4 μM•hr, with an average concentration of 2.7 μM. The average concentration exceeded the IC_{50} values of RIF obtained with monkey hepatocytes and cOATP-expressing HEK-293 cells. The RIF systemic exposures obtained in the present study were comparable to those reported in patients at a therapeutic dose (Acocella et al., 1985; Sanofi-Aventis, 2005) and in monkeys following a 18 mg/kg dose (Prueksaritanont et al., 2006).

IVIVE-Based Prediction of DDI Between RSV and RIF Involving the Inhibition of OATPs. An IVIVE exercise was conducted to assess the relevance of *in vitro* IC_{50} values to the prediction of the OATP-mediated DDI between RSV and RIF in cynomolgus monkeys and humans, and the results are summarized in Table 6. For the human DDI between RSV and RIF, J. Polli and his colleagues at GlaxoSmithKine found that the coadministration of a single-dose (600-mg) of RIF caused a 3-fold increase in the AUC of RSV (10 mg) in 11 healthy subjects (J. Polli, personal communication). This clinical observation was used to support the IVIVE exercise described herein.

Three equation-based approaches and different types of free and total inhibitor concentrations (i.e., I_{max}, I_{ave}, and $I_{in,max}$) were explored in the IVIVE. Among the 3 equations used, Eq. 1 yielded the highest predictions of AUC ratio (Table 6), because of the assumption that OATP-mediated active uptake accounts for 100% of RSV clearance. As expected, when the fraction of OATP-mediated clearance was taken into consideration (Eqs. 2 and 3), the predicted AUC ratios were markedly reduced and fell within two-fold of the observed AUC ratio in both

JPET Fast Forward. Published on January 7, 2013 as DOI: 10.1124/jpet.112.200691
This article has not been copyedited and formatted. The final version may differ from this version.

monkeys and humans. For the types of inhibitor concentrations used in the IVIVE, the $I_{in,max}$ approach provided the most conservative (i.e., highest) estimate on the change of the AUC ratio (Table 6). Protein binding also had the most significant effect on the AUC ratio when Eq. 1 was used (>5-fold difference between the free and total inhibitor concentrations). Less pronounced effects were observed when Eqs. 2 and 3 were applied. In general, when protein binding was taken into account, the magnitude of effect of RIF on RSV AUC (Eqs. 2 and 3) was under-predicted.

In the following, we investigated if the predicted AUC ratio in monkeys could be used to calibrate the prediction of clinical DDIs (Fig. 5). For this purpose, a total of 18 different monkey IVIVE permutations were attempted based on three models with different input for inhibitor concentration. Overall, the trend for monkey was similar to that of human with respect to IVIVE (Fig. 5 and Supplementary Fig. 5). There was good correlation between monkey and human predicted AUC ratios (R^2 = 0.98). Based on monkey IVIVE, 12 permutations rendered a DDI (AUC ratio) prediction that fell within the AUC ratio range specified by the 90% CI in monkey. If the same 12 IVIVE approaches were used for the human *in vitro* data, they would have predicted an AUC ratio that ranged from 1.81 to 3.16. The 1.81 to 3.16 range compares favorably with the observed human AUC ratio 90% CI (i.e., 2.51 to 3.52). In fact, 4 of the 12 permutations rendered a predicted human AUC ratio that fell at/within the 90% CI.

JPET Fast Forward. Published on January 7, 2013 as DOI: 10.1124/jpet.112.200691
This article has not been copyedited and formatted. The final version may differ from this version.

Discussion

OATPs are expressed at the sinusoidal membrane of hepatocytes and play a critical role in drug elimination (Giacomini et al., 2010; Niemi et al., 2011; Yoshida et al., 2012). They also serve as the loci of important DDIs. As high-throughput OATP inhibition screening becomes more routine (Gui et al., 2010; Soars et al., 2012), an increasing number of new chemical entities will be identified as inhibitors. Such a scenario will necessitate tier-based screening funnels to support compound selection. To this end, the cynomolgus monkey was evaluated as a potential model for studying OATP-mediated DDIs in order to complement existing inhibition screening and facilitate IVIVE-based DDI risk assessment and decision making (Fig. 1).

In the present work, the cloning of cOATP1B1, cOATP1B3, and cOATP2B1 revealed that the amino acid sequences were similar to their corresponding human orthologs (91.9, 93.5 and 96.6%, respectively) and almost identical to the corresponding rhesus counterparts (99.9, 99.3 and 99.9%, respectively). These data suggest that cynomolgus monkeys may be a good model for studying OATP-mediated DDIs in humans.

In order to explore substrate specificity and compare inhibitor potency between human and monkey hepatic OATP transporters, cOATP1B1, cOATP1B3, and cOATP2B1 were independently expressed in HEK-293 cells. Based on the results obtained with the three chosen substrates (E17βG, CCK-8, and E3S), it is concluded that cOATPs and hOATPs are qualitatively similar. Such a conclusion is partially supported by the fact that 4 amino acids (Asp70, Phe73, Glu74, and Gly76) located in the transmembrane domain 2 of OATP1B1 are essential to its transport function (Li et al., 2012), and a sequence alignment analysis showed that these 4 amino acid positions are identical between humans and cynomolgus monkeys for both OATP1B1 and

JPET Fast Forward. Published on January 7, 2013 as DOI: 10.1124/jpet.112.200691
This article has not been copyedited and formatted. The final version may differ from this version.

OATP1B3. However, a more quantitative comparison (across different OATPs) requires expression data for each OATP protein in the individual cell lines. This is particularly true when attempting to define substrate specificity. For example, in the present study, the rate of E3S uptake was greatest with OATP2B1 vs. OATP1B1 and OATP1B3. In the literature, E3S was initially found to be selective for OATP1B1 relative to OATP1B3 (Hirano et al, 2004). The same investigators subsequently found that E3S was also a substrate of OATP2B1 (Hirano et al., 2006), which was corroborated by others (Noe et al., 2007; Satoh et al., 2005; Kis et al., 2010; Shirasaka et al., 2012; Koenen et al. 2012). For the different OATPs, therefore, assignment of substrate specificity requires well defined assay conditions (e.g., linearity), in addition to kinetic parameters and quantitation of individual OATP proteins in different expression systems. From the standpoint of inhibition, the IC_{50} values between cOATPs and hOATPs were in a good concordance (less than 3-fold difference, Table 2 and Fig. 3). Taken together, these results suggest that cOATPs have transport characteristics comparable to those of hOATPs.

To extend our findings from *in vitro* to *in vivo*, RSV and RIF, a known hOATP substrate-inhibitor pair, were selected to evaluate an OATP-based DDI in cynomolgus monkeys. The *in vitro* transport parameters (K_m and IC_{50}) generated with cOATPs and primary cynomolgus monkey hepatocytes were comparable to those derived with hOATPs and human primary hepatocytes. Consistently, the AUC of RSV in cynomolgus monkeys was increased 2.9-fold following a single oral coadministration of RIF and RSV (15 and 3 mg/kg, respectively). A similar increase (3-fold) in RSV AUC caused by a single RIF dose has been observed in human subjects (J. Polli, Glaxo-Smith Kline, personal communication), demonstrating the relevance of the RSV-RIF DDI in monkeys both *in vitro* and *in vivo*. It is important to note that the pharmacokinetic profile of RSV has been characterized after coadministeration of multiple doses

JPET Fast Forward. Published on January 7, 2013 as DOI: 10.1124/jpet.112.200691
This article has not been copyedited and formatted. The final version may differ from this version.

of RIF in healthy male volunteers (Zhang et al., 2008). In this stance, the AUC of RSV was not significantly altered because of the likely opposing effects of RIF-mediated CYP2C9 induction and OATP transporter inhibition.

In the present study, RSV was selected as a probe substrate because of its transport kinetics and pharmacokinetic properties: (1) RSV is a OATP1B1, OATP1B3, and OATP2B1 substrate; (2) The relative contributions of hOATP1B1 and hOATP1B3 to RSV hepatic clearance are known (Kitamura et al. 2008); (3) Active transport clearance of RSV dominates the entry into hepatocytes at therapeutic concentrations (Table 3 and Supplementary Fig. 2); (4) RSV undergoes relatively little metabolism, which avoids the complication of P450-mediated DDIs (Kitamura et al., 2008; Martin et al., 2003c); (5) Human radiolabeled data for RSV are available, allowing the fraction of various elimination pathways to be clearly defined (Martin et al., 2003b and 2003c). It should be pointed out that, in this case, the contribution of hOATP2B1 was negligible because of its relatively low protein expression in human hepatocytes (Kitamura et al., 2008). In addition, our inhibition studies indicated that the IC_{50} values (81.6 to 89.8 μM) of RIF for hOATP2B1 and cOATP2B1 were significantly higher than its therapeutically relevant concentrations (≤ 10 μM), excluding the significant role of OATP2B1 in the drug interaction caused by RIF.

Three equation-based approaches, in addition to a consideration of free and total inhibitor concentrations, were explored in the RIF-RSV DDI IVIVE exercise. Theoretically, it is expected that Eq. 1 that assumes the entire clearance pathway affected by an inhibitor, together with a total $I_{in,max}$, leads to the largest predicted AUC ratio. On the other hand, Eqs. 2 or 3 that consider only a portion of the elimination pathways affected by the inhibitor, together with a free I_{ave}, should yield the lowest predicted AUC ratio. Therefore, it is difficult to determine which equation to

use prospectively in order to gauge the risk of a DDI involving inhibition of OATP. For a substrate, the accuracy of DDI predictions depends on the sound understanding of elimination pathways and the fraction of clearance pathways affected by the inhibitor, as demonstrated in the current IVIVE exercise. For an inhibitor, the accuracy of DDI assessment, using equation-based approaches, is governed by the inhibitor (free or total) concentrations used. As shown in Table 6, use of Eq. 2 or 3 (with free inhibitor concentration) somewhat underestimated the true extent of the DDI between RSV and RIF. However, the predictions were still within 2-fold of the observed result.

Employing cynomolgus monkeys as a potential model for studying OATP-mediated DDIs is an important step towards the understanding the relevance of the *in vitro* data to the *in vivo* situation. Several studies have clearly shown the caveats associated with using *in vitro* data alone for predicting OATP-mediated DDIs (Hinton et al., 2008; Imamura et al., 2011; Karlgren et al., 2012; Yoshida et al., 2012). The general approach recommended by the recent FDA draft DDI Guidance for Industry, as well as the article by the ITC Technical Working Group (Giacomini et al., 2010), provides a sound approach to assess the OATP-mediated DDI risk. But the conservative approach (i.e., Eq. 1) tends to forecast a higher DDI risk. From a drug discovery point of view, there is a need to balance the risk with such an approach in order to minimize the premature termination of good compounds. This is particularly important as high-throughput OATP inhibition screens become prevalent in the industry. To this end, cynomolgus monkey may serve as a model to support an IVIVE exercise. This, together with a sound understanding of species difference in the *in vitro* OATP profile (cynomolgus monkey versus human), would form the basis of a strategy to support OATP-related DDI risk assessment prior to first in man (Fig. 1). As described herein, it was possible to study a well known hOATP

JPET Fast Forward. Published on January 7, 2013 as DOI: 10.1124/jpet.112.200691
This article has not been copyedited and formatted. The final version may differ from this version.

inhibitor-substrate pair (RIF-RSV) in the monkey. Importantly, the rank order of the predictions in monkeys was comparable to that in humans (Fig. 5), and there was a good correlation between monkey and human IVIVE (R^2 = 0.98, data not shown). Twelve out of 18 permutations rendered AUC ratios that fell within the AUC ratio range specified by the 90% CI in monkeys. If the same 12 IVIVE approaches were supported by the human *in vitro* data, they would have predicted an AUC ratio that compared favorably with the observed human AUC ratio. Although only 1 substrate-inhibitor pair was evaluated in the present work, the results illustrated that the approach could be used to support risk assessment prior to first in man.

To implement the strategy outlined above, one could envision two possible schemes (Fig. 1, scenario 3). For a new chemical entity that is an inhibitor of OATPs *in vitro*, the approach may be readily applicable in a drug discovery setting, where compound prioritization and defining the extent of OATP inhibition is more critical in support of lead optimization. The key in this case is to ensure that the OATP inhibition caused by the new chemical entity is evident in the *in vitro* systems of monkeys and the concentration corresponding to the *in vitro* IC_{50} (or K_i) can be readily attained *in vivo* (e.g., plasma) for testing the DDI potential in monkeys. Based on the outcome of an *in vivo* monkey DDI study, one could then use various IVIVE constructs (including physiologically-based pharmacokinetic modeling) to bridge the *in vitro* and *in vivo* findings in monkeys and apply the same construct to the human situation, assuming that human pharmacokinetics can reasonably be predicted and OATP-mediated DDIs are driven by inhibitor concentrations in the circulation. It is also important to consider any difference between monkeys and humans with respect to the *in vitro* metabolite profile and inhibition of potential circulating metabolites. For a new chemical entity that is a substrate of OATPs, the strategy may only be useful if there is a clear understanding of its disposition in monkeys and humans. Such

information would support a more quantitative assessment of DDI risk. In this instance, it is important to determine if OATPs play a comparable role in the disposition of the compound in both species, which likely requires the use of a radiolabel. Specifically, the importance of OATP-mediated uptake clearance (relative to total hepatic clearance), as well as the fraction of total body clearance that undergoes hepatic, renal, and other elimination pathways, needs to be understood in both species. In addition, the consideration of using a monkey DDI study for the IVIVE calibration needs to be balanced with the risk and benefit of directly conducting a human DDI study, which depends on the need and stage of a clinical program.

In summary, a cynomolgus monkey OATP DDI model was successfully developed. For the first time, 3 cOATPs (cOATP1B1, cOATP1B3, and cOATP2B1) were characterized in terms of their substrate specificity and inhibition, and relatively minimal differences (vs. hOATPs) were demonstrated. Furthermore, cOATP1B1 and cOATP1B3 were susceptible to inhibition by RIF, resembling the observations with hOATP1B1 and hOATP1B3. With the use of RSV as an *in vivo* probe substrate and RIF as an inhibitor for cOATPs, the pharmacokinetic consequence of the *in vitro* findings was demonstrated in cynomolgus monkeys, with a result comparable to that in humans. Various IVIVE approaches for predicting the RSV-RIF DDI were further explored in cynomolgus monkeys and humans. Therefore, RSV and RIF can be used as clinically relevant *in vitro* and *in vivo* probes to study OATP activity and inhibition, respectively, in cynomolgus monkeys. Collectively, the results described herein demonstrate that the cynomolgus monkey has the potential to serve as a useful model to support the assessment of OATP-mediated DDIs and to facilitate IVIVE exercises employing *in vitro* hOATP data.

JPET Fast Forward. Published on January 7, 2013 as DOI: 10.1124/jpet.112.200691
This article has not been copyedited and formatted. The final version may differ from this version.

Acknowledgments

The authors wish to thank Joseph W. Polli Ph.D (GlaxoSmithKline, Research Triangle Park, NC) for providing the single dose clinical RSV-RIF DDI data described in the manuscript. The data had been presented previously at the Second International Transporter Consortium Workshop (ITCW2), Membrane Transporters in Drug Development: Best Practices and Future Directions (March 12-13, 2012; National Harbor, MD).

Authorship Contributions

Participated in research design: Shen, Yang, Mintier, Balimane, Jemal, Marathe and Rodrigues.

Conducted experiments: Shen, Han, Chen, Zhao, Zhang, Kallipatti, Selvam, Sukrutharaj and Krishnamurthy.

Contributed new reagents or analytic tools: Shen, Mintier, Zhang and Jemal.

Performed data analysis: Shen, Mintier, Yang and Rodrigues.

Wrote or contributed to the writing of the manuscript: Shen, Yang and Rodrigues.

Other: None.

JPET Fast Forward. Published on January 7, 2013 as DOI: 10.1124/jpet.112.200691
This article has not been copyedited and formatted. The final version may differ from this version.

References

Acocella G (1978) Clinical pharmacokinetics of rifampicin. *Clin Pharmacokinet* **3**:108-127.

Acocella G, Conti R, Luisetti M, Pozzi E, and Grassi C (1985) Pharmacokinetic studies on antituberculosis regimens in humans. I. Absorption and metabolism of the compounds used in the initial intensive phase of the short-course regimens: single administration study. *Am Rev Respir Dis* **132**:510-515.

Akabane T, Tabata K, Kadono K, Sakuda S, Terashita S, and Teramura T (2010) A comparison of pharmacokinetics between humans and monkeys. *Drug Metab Dispos* **38**:308-316.

Ebeling M, Küng E, See A, Broger C, Steiner G, Berrera M, Heckel T, Iniguez L, Albert T, Schmucki R, Biller H, Singer T, and Certa U (2011) Genome-based analysis of the nonhuman primate Macaca fascicularis as a model for drug safety assessment. *Genome Res* **10**:1746-1756.

European Medicines Agency, Science Medicines Health, Committee for Human Medicinal Products (CHMP). Guideline on the Investigation of Drug Interactions. *EMA website http://www.ema.europa.eu/docs/en_GB/document_library/Scientific_guideline/2012/07/WC500129606.pdf,* (2012)

Fenner KS, Jones HM, Ullah M, Kempshall S, Dickins M, Lai Y, Morgan P, and Barton HA (2012) The evolution of the OATP hepatic uptake transport protein family in DMPK sciences: from obscure liver transporters to key determinants of hepatobiliary clearance. *Xenobiotica* **42**:28-45.

Giacomini KM, Huang SM, Tweedie DJ, Benet LZ, Brouwer KL, Chu X, Dahlin A, Evers R, Fischer V, Hillgren KM, Hoffmaster KA, Ishikawa T, Keppler D, Kim RB, Lee CA, Niemi M, Polli JW, Sugiyama Y, Swaan PW, Ware JA, Wright SH, Yee SW, Zamek-

Gliszczynski MJ, and Zhang L (2010) Membrane transporters in drug development. *Nature Rev Drug Discov* **9**:215–236.

Gui C, Obaidat A, Chaguturu R, and Hagenbuch B (2010) Development of a cell-based high-throughput assay to screen for inhibitors of organic anion transporting polypeptides 1B1 and 1B3. *Curr Chem Genomics* **4**:1-8.

Han YH, Busler D, Hong Y, Tian Y, Chen C, and Rodrigues AD (2010) Transporter studies with the 3-O-sulfate conjugate of 17alpha-ethinylestradiol: assessment of human liver drug transporters. *Drug Metab Dispos* **38**:1072-1082.

Hinton LK, Galetin A, and Houston JB (2008) Multiple inhibition mechanisms and prediction of drug-drug interactions: status of metabolism and transporter models as exemplified by gemfibrozil-drug interactions. *Pharm Res* **25:**1063–1074.

Hirano M, Maeda K, Shitara Y, and Sugiyama Y (2004) Contribution of OATP2 (OATP1B1) and OATP8 (OATP1B3) to the hepatic uptake of pitavastatin in humans. *J Pharmacol Exp Ther* **311**:139-146.

Hirano M, Maeda K, Shitara Y, and Sugiyama Y (2006) Drug-drug interaction between pitavastatin and various drugs via OATP1B1. *Drug Metab Dispos* **34**:1229-1236.

Imamura Y, Murayama N, Okudaira N, Kurihara A, Okazaki O, Izumi T, Inoue K, Yuasa H, Kusuhara H, and Sugiyama Y (2011) Prediction of fluoroquinolone-induced elevation in serum creatinine levels: a case of drug-endogenous substance interaction involving the inhibition of renal secretion. *Clin Pharmacol Ther* **89:**81–88.

Iwasaki K and Uno Y (2009) Cynomolgus monkey CYPs: a comparison with human CYPs. *Xenobiotica* **39**:578–581.

Kantola T, Kivistö KT, and Neuvonen PJ (1998). Effect of itraconazole on the pharmacokinetics of atorvastatin. *Clin Pharmacol Ther* **64**:58–65.

Karlgren M, Ahlin G, Bergström CA, Svensson R, Palm J, and Artursson P (2012) *In vitro* and in silico strategies to identify OATP1B1 inhibitors and predict clinical drug-drug interactions. *Pharm Res* **29**:411–426.

Kis O, Zastre JA, Ramaswamy M, Bendayan R (2010) pH dependence of organic anion-transporting polypeptide 2B1 in Caco-2 cells: potential role in antiretroviral drug oral bioavailability and drug-drug interactions. *J Pharmacol Exp Ther* **334**:1009-1022.

Kitamura S, Maeda K, Wang Y, and Sugiyama Y (2008) Involvement of multiple transporters in the hepatobiliary transport of rosuvastatin. *Drug Metab Dispos* **36**:2014-2023.

Koenen A, Köck K, Keiser M, Siegmund W, Kroemer HK, Grube M (2012) Steroid hormones specifically modify the activity of organic anion transporting polypeptides. *Eur J Pharm Sci* **47**:774-780.

Lemahieu WP, Hermann M, Asberg A, Verbeke K, Holdaas H, Vanrenterghem Y, and Maes BD (2005) Combined therapy with atorvastatin and calcineurin inhibitors: no interactions with tacrolimus. *Am J Transplant* **5**:2236-2243.

Li N, Hong W, Huang H, Lu H, Lin G, Hong M (2012) Identification of amino acids essential for estrone-3-sulfate transport within transmembrane domain 2 of organic anion transporting polypeptide 1B1. *PLoS One* **7**:e36647.

Maeda K and Sugiyama Y (2010) Comparison of the function of transporters involved in the hepatic and renal uptake of drugs between monkeys and humans. *PSJAP Annual meeting* Okayama, Japan.

Martin PD, Warwick MJ, Dane AL, and Cantarini VC (2003a) A double-blind, randomized, incomplete crossover trial to assess the dose proportionality of rosuvastatin in healthy volunteers. *Clin Ther* **25**:2215-2224.

Martin PD, Warwick MJ, Dane AL, Brindley C, and Short T (2003b) Absolute oral bioavailability of rosuvastatin in healthy white adult male volunteers. *Clin Ther* **25**:2553-2563.

Martin PD, Warwick MJ, Dane AL, Hill SJ, Giles PB, Phillips PJ, and Lenz E (2003c) Metabolism, excretion, and pharmacokinetics of rosuvastatin in healthy adult male volunteers. *Clin Ther* **25**:2822-2835.

Mazzu AL, Lasseter KC, Shamblen EC, Agarwal V, Lettieri J and Sundaresen P (2000) Itraconazole alters the pharmacokinetics of atorvastatin to a greater extent than either cerivastatin or pravastatin. *Clin Pharmacol Ther* **68**:391–400.

Mehta J, Gandhi IS, Sane SB, and Wamburkar MN (1985) Effect of clofazimine and dapsone on rifampicin (Lositril) pharmacokinetics in multibacillary and paucibacillary leprosy cases. *Indian J Lepr* **57**:297-310.

Niemi M, Pasanen MK, and Neuvonen PJ (2011) Organic anion transporting polypeptide 1B1: a genetically polymorphic transporter of major importance for hepatic drug uptake. *Pharmacolo Rev* **63**:157-181.

Noe J, Portmann R, Brun ME, Funk C (2007) Substrate-dependent drug-drug interactions between gemfibrozil, fluvastatin and other organic anion-transporting peptide (OATP) substrates on OATP1B1, OATP2B1, and OATP1B3. *Drug Metab Dispos* **35**:1308-1314.

Prueksaritanont T, Kuo Y, Tang C, Li C, Qiu Y, Lu B, Strong-Basalyga K, Richards K, Carr B, and Lin JH (2006) *In vitro* and *in vivo* CYP3A64 induction and inhibition studies in rhesus

monkeys: a preclinical approach for CYP3A-mediated drug interaction studies. *Drug Metab Dispos* **34**:1546-1555.

Sanofi-Aventis (2005) Prescribing information on Rafadin (Rifampin), in *Physicians' Desk Reference*, vol **59**, pp 736-739, Medical Economics Co., Montvale, NJ.

Satoh H, Yamashita F, Tsujimoto M, Murakami H, Koyabu N, Ohtani H, Sawada Y (2005) Citrus juices inhibit the function of human organic anion-transporting polypeptide OATP-B. *Drug Metab Dispos* **33**:518-523.

Shen H, Lee FY, and Gan J (2011) Ixabepilone, a novel microtubule-targeting agent for breast cancer, is a substrate for P-glycoprotein (P-gp/MDR1/ABCB1) but not breast cancer resistance protein (BCRP/ABCG2). *J Pharmacol Exp Ther* **337**:423–432.

Shirasaka Y, Mori T, Shichiri M, Nakanishi T, Tamai I (2012) Functional pleiotropy of organic anion transporting polypeptide OATP2B1 due to multiple binding sites. *Drug Metab Pharmacokinet* **27**:360-364.

Soars MG, Barton P, Ismair M, Jupp R, and Riley RJ (2012) The Development, Characterization and Application of an OATP1B1 Inhibition Assay in Drug Discovery. *Drug Metab Dispos* **40**:1641-1648.

Tang C and Prueksaritanont T (2010) Use of *in vivo* animal models to assess pharmacokinetic drug-drug interactions. *Pharm Res* **27**:1772-1787.

Tahara H, Shono M, Kusuhara H, Kinoshita H, Fuse E, Takadate A, Otagiri M, Sugiyama Y (2005) Molecular cloning and functional analyses of OAT1 and OAT3 from cynomolgus monkey kidney. *Pharm Res* **22**:647-660.

US Department of Health and Human Services, Food and Drug Administration, Center for Drug Evaluation and Research (CDER), Center for Biologics Evaluation and Research (CBER).

Guidance for Industry. Drug Interaction Studies — Study Design, Data Analysis, and Implications for Dosing and Labeling. *US FDA website http://www.fda.gov/downloads/Drugs/GuidanceComplianceRegulatoryInformation/Guidances/UCM292362.pdf*, (2012).

Vuppugalla R, Kim S, Zvyaga T, Han Y-H, Balimane P, Marathe P and Rodrigues AD (2010) Anticipating and minimizing drug interactions in a drug discovery and development setting: an industrial perspective, in *Enzyme- and Transporter-Based Drug-Drug Interactions: Progress and Future Challenges* (Pang KS, Rodrigues AD, Peter RM eds), pp 585-624, Springer, New York.

White EP, Pimprale S, Yu Z, Ketty V, Bourgea J, Patten CJ, Crespi C and Xiao G (2006) Cloning and characterization of cynomolgus monkey and rhesus monkey organic anion transporting poloypeptide 1B3 and comparison of their function with human OATP-1B3. *AAPS Annual meeting and exposition*, San Antonio, TX.

Yabe Y, Galetin A, and Houston JB (2011) Kinetic characterization of rat hepatic uptake of 16 actively transported drugs. *Drug Metab Dispos* **39**:1808-1814.

Yasunaga M, Takemura M, Fujita K, Yabuuchi H, Wada M (2008) Molecular cloning and functional characterization of cynomolgus monkey multidrug resistance-associated protein 2 (MRP2). *Eur J Pharm Sci* **35**:326-334.

Yoshida K, Maeda K, and Sugiyama Y (2012) Transporter-mediated drug-drug interactions involving OATP substrates: predictions based on *in vitro* inhibition studies. *Clin Pharmacol Ther* doi: 10.1038/clpt.2011.351.

Zhang W, Deng S, Chen XP, Zhou G, Xie HT, He FY, Cao D, Li YJ, Zhou HH (2008) Pharmacokinetics of rosuvastatin when coadministered with rifampicin in healthy males: a randomized, single-blind, placebo-controlled, crossover study. *Clin Ther* **30**:1283-1289.

Footnotes

Reprint requests: Hong Shen, F1.3811, Route 206 & Province Line Road., Bristol-Myers Squibb Company, Princeton, NJ 08543. Telephone: (609) 252-4509; Facsimile: (609) 252-6802

This study is supported by Bristol-Myers Squibb Company.

JPET Fast Forward. Published on January 7, 2013 as DOI: 10.1124/jpet.112.200691
This article has not been copyedited and formatted. The final version may differ from this version.

Figure Legends

Fig. 1. Idealized approach for the assessment of OATP DDI potential. In scenario 1, clinical DDI assessment is conducted because of *in vitro* results only (e.g., IC_{50} is low; < 1 μM). No attempt is made to predict the DDI. In the second scenario, *in vitro* human data are used to (semi)quantitatively predict the DDI. Information such as free fraction (f_u), inhibitor concentration (e.g., I_{max}, I_{ave}, $I_{in,max}$) and projected (or known) human pharmacokinetic profile is considered (see *Materials and Methods*). In scenario 3, there are two possible schemes. For an inhibitor, *in vitro* cynomolgus data are generated and compared to human data (IC_{50} or K_i, f_u, etc). It may be necessary to consider any metabolites that are formed *in vitro*, assess them as OATP inhibitors also, and include them in the IVIVE exercise. For a substrate, in addition to the *in vitro* J_{max} (V_{max}) and K_m comparison (monkey vs. human), one needs to understand the importance and species-dependent differences in OATP-mediated uptake clearance (relative to total hepatic clearance), and the contribution of hepatic, renal and other elimination pathways to total body clearance. Based on the comparison, a decision is made as to the validity of the cynomolgus monkey as a DDI model. If a clinically relevant dose (and exposure) is achievable in the cynomolgus monkey for an OATP substrate, or concentrations are attainable to cover the K_i or IC_{50} for an OATP inhibitor, an *in vivo* DDI monkey study may be initiated. In parallel, the extent of the DDI in the monkey is predicted using various IVIVE approaches (e.g., f_u-corrected vs f_u-uncorrected IVIVE, I_{max}-, I_{ave}-, or $I_{in,max}$-based IVIVE, physiologically-based pharmacokinetic modeling (PBPK), etc). Subsequently, the observed victim AUC ratio is compared to the predicted victim AUC ratio. The success of the IVIVE exercise is assessed and whichever approach yields the best IVIVE is then used to support the prediction of the OATP-

JPET Fast Forward. Published on January 7, 2013 as DOI: 10.1124/jpet.112.200691
This article has not been copyedited and formatted. The final version may differ from this version.

mediated DDI in human subjects. In scenario 3, the monkey IVIVE is used to "calibrate" the human IVIVE.

Fig. 2. Uptake of [^{3}H] E17βG (1 μM) (A), [^{3}H]CCK-8 (0.1 μM) (B), and [^{3}H]E3S (1 μM) (C) into mock-, OATP1B1-, OATP1B3-, and OATP2B1-expressing HEK-293 cells was determined after 1.5 min of incubation. Data are expressed as mean ± SD (n = 3 determinations). *$p < 0.05$, uptake by OATP-expressing cells compared with the uptake by mock cells.

Fig. 3. Comparison of 6 compounds (RIF, CsA, verapamil, ritonavir, gemfibrozil and saquinavir) as inhibitors of cOATPs and hOATPs (IC_{50}s reported in Table 2). The solid and dotted lines represent the line of unity and the 33 to 300% range of the observed IC_{50}, respectively.

Fig. 4. Mean plasma concentration-time profile of RSV in cynomolgus monkeys after a single oral dose of RSV (3 mg/kg) and following a single oral dose of RSV (3 mg/kg) with oral RIF (15 mg/kg). RIF was dosed one hour ahead of RSV (A). Mean plasma concentration-time profile of RIF in cynomolgus monkeys after an oral dose of 15 mg/kg (B). Data are expressed as mean ± SD (n = 3 animals).

Fig. 5. Predicted change in RSV exposure (AUC ratio) in humans calibrated with IVIVE in monkeys. The calculated AUC ratios were obtained by applying different equations with different types of free and total inhibitor concentrations (i.e., I_{max}, I_{ave}, and $I_{in,max}$). All predicted

JPET Fast Forward. Published on January 7, 2013 as DOI: 10.1124/jpet.112.200691
This article has not been copyedited and formatted. The final version may differ from this version.

and observed AUC ratios in monkeys and humans, as well as the corresponding 90% confidence interval (CI), can be found in Table 6.

Table 1

Amino acid sequence identity between cynomolgus monkey, rhesus monkey and human OATPs

	Cynomolgus Monkey (%)			Rhesus Monkey (%)			Human (%)		
	cOATP1B1	**cOATP1B3**	**cOATP2B1**	**rOATP1B1**	**rOATP1B3**	**rOATP2B1**	**hOATP1B1**	**hOATP1B3**	**hOATP2B1**
cOATP1B1	100	76.7	27.2	99.9			91.9		
cOATP1B3		100	27.5		99.3			93.5	
cOATP2B1			100			99.9			96.6

Table 1 Legend:

The percentages of identity among the various sequences were determined from the amino acid alignment reported in Supplementary Figure 1.

Table 2

Inhibition of individually-expressed cOATPs and hOATPs in HEK-293 cells

	IC_{50} (μM)[d]					
Compound	**cOATP1B1[a]**	**hOATP1B1[a]**	**cOATP1B3[b]**	**hOATP1B3[b]**	**cOATP2B1[c]**	**hOATP2B1[c]**
RIF	0.20 ± 0.08	0.55 ± 0.07	1.4 ± 0.5	0.46 ± 0.13	69.1 ± 7.5	40.1 ± 5.1
CsA	1.0 ± 0.3	0.87 ± 0.29	0.50 ± 0.11	0.80 ± 0.22	> 50	> 50
Ritonavir	0.49 ± 0.14	1.3 ± 0.3	1.3 ± 0.6	4.0 ± 1.1	4.5 ± 1.8	10.7 ± 2.3
Gemfibrozil	20.2 ± 5.8	41.4 ± 9.0	22.4 ± 6.6	50.1 ± 27.3	> 100	> 100
Verapamil	13.5 ± 2.8	14.8 ± 3.1	52.7 ± 15.9	87.3 ± 35.8	> 200	> 200
Saquinavir	2.9 ± 0.9	1.6 ± 0.4	3.6 ± 1.5	5.5 ± 3.0	12.3 ± 4.8	9.4 ± 3.2

Table 2 Legend:

[a]IC_{50} determined at a final E17βG concentration of 1 μM.

[b]IC_{50} determined at a final CCK-8 concentration of 0.1 μM.

[c]IC_{50} determined at a final E3S concentration of 1 μM.

[d]Values represent the mean ± SD (n = 3 to 4 determinations).

Table 3

Kinetic parameters describing the uptake of RSV into cynomolgus monkey and human primary hepatocytes and OATP-expressing HEK-293 cells

	Hepatocytes[a]	
	Cynomolgus Monkey	**Human**
K_m (μM)	6.7 ± 0.8	10.3 ± 1.9
V_{max} (pmoL/min/10^6cells)	172.3 ± 9.5	114.3 ± 11.6
V_{max}/K_m (μl/min/10^6cells)	25.7	11.0
P_{diff} (μl/min/10^6cells)	0.7 ± 0.1	0.5 ± 0.1
$[(V_{max}/K_m)/(V_{max}/K_m + P_{diff})]\cdot 100\%$[b]	97	96

	HEK-293 Cells[a,c]					
	cOATP1B1	**hOATP1B1**	**cOATP1B3**	**hOATP1B3**	**cOATP2B1**	**hOATP2B1**
K_m (μM)	14.4 ± 3.0	15.3 ± 3.0	14.5 ± 2.0	13.5 ± 2.0	9.6 ± 0.8	10.6 ± 1.0

Table 3 Legend:

[a]Data represent mean ± SD of the parameter estimate after non-linear fitting of the data (see *Materials and Methods*).

[b]Data indicate that > 95% of total uptake is mediated by active transport.

[c]V_{max} values of RSV uptake into OATP-expressing HEK-293 cells are not reported in the absence of specific OATP protein expression data.

JPET Fast Forward. Published on January 7, 2013 as DOI: 10.1124/jpet.112.200691
This article has not been copyedited and formatted. The final version may differ from this version.

Table 4

RIF as an inhibitor of RSV uptake into hepatocytes and HEK-293 cells expressing individual OATPs

	IC_{50} (μM)[a]			
	Hepatocytes	**OATP1B1**	**OATP1B3**	**OATP2B1**
Cynomolgus Monkey	0.28 ± 0.16	0.42 ± 0.09	1.69 ± 0.28	81.6 ± 15.2
Human	0.90 ± 0.45	1.10 ± 0.28	0.49 ± 0.13	89.8 ± 5.4

JPET Fast Forward. Published on January 7, 2013 as DOI: 10.1124/jpet.112.200691
This article has not been copyedited and formatted. The final version may differ from this version.

Table 4 Legend:

[a]IC_{50} values were generated at a low concentration of RSV (0.1 μM) and data are represented as the mean ± SD (n = 3 to 4 determinations) (see *Materials and Methods*).

Table 5

Pharmacokinetic parameters of RSV after oral administration of RSV (3 mg/kg) to cynomolgus monkeys dosed with and without RIF (15 mg/kg PO single dose)

Analyte	Parameter	Control (RSV Alone)	RIF-Treatment[a]	Ratio[b]	90% CI
RSV	C_{max} (nM)	16.4 ± 11.7	113.2 ± 29.0	10.23 ± 8.60 (7.15, 3.59 and 19.95)[d]	1.87-34.26
	$AUC_{0\text{-}last}$ (nM•hr)	160 ± 99	419 ± 108	3.04 ± 1.25	1.44-5.72
	$AUC_{0\text{-}inf}$ (nM•hr)	176 ± 109	439 ± 110	2.89 ± 1.11 (2.74, 1.86 and 4.06)[d]	1.42-5.31
	t_{max} (hr)	5.0 (5.0, 5.0 and 5.0)[c]	1.0 (1.0, 1.0 and 1.0)[c]	0.2 ± 0.0	
	$t_{1/2}$ (hr)	6.1 ± 0.3	5.8 ± 1.1	0.96 ± 0.22	0.64-1.39
RIF	C_{max} (µM)		9.2 ± 2.5		
	C_{last} (µM)		0.19 ± 0.16		
	$AUC_{0\text{-}last}$ (µM•hr)		67.4 ± 14.9		
	t_{max} (hr)		3.3 ± 0.6		
	$t_{1/2}$ (hr)		3.7 ± 0.5		

Legend to Table 5:

Data reported as mean ± SD, n = 3 different animals.

[a]RIF was dosed one hr prior to RSV

[b]Represents the parameter ratio (+RIF/-RIF)

[c]Mean (individual value)

[d]Mean ± SD (individual value)

Table 6

Observed and predicted RSV AUC ratios with RIF as inhibitor in cynomolgus monkeys and humans

Species	AUC Ratio (Observed)	90% CI of AUC Ratio	AUC Ratio (Predicted)						
			Prediction Method[a]	I_{max}		I_{ave}		$I_{in,max}$	
				Total	Free	Total	Free	Total	Free
Cynomolgus Monkey	2.89	1.42-5.31	Eq. 1	33.93	7.26	11.04	2.91	63.04	12.79[b]
Human	3.00	2.51-3.52		9.51	2.70	5.06	1.81	19.72	4.74[b]
Cynomolgus Monkey	2.89	1.42-5.31	Eq. 2	3.32	2.64	2.90	1.90	3.43	2.97
Human	3.00	2.51-3.52		2.81	1.83	2.37	1.48	3.16	2.32
Cynomolgus Monkey	2.89	1.42-5.31	Eq. 3	3.03	2.13	2.41	1.54	3.25	2.51
Human	3.00	2.51-3.52		2.78	1.81	2.34	1.47	3.14	2.29

Legend to Table 6

[a]Fold AUC change predicted using different methods or equations (see *Materials and Methods*).

[b]Calculated *R*-value using the approach recommended by Food and Drug Administration and ITC.

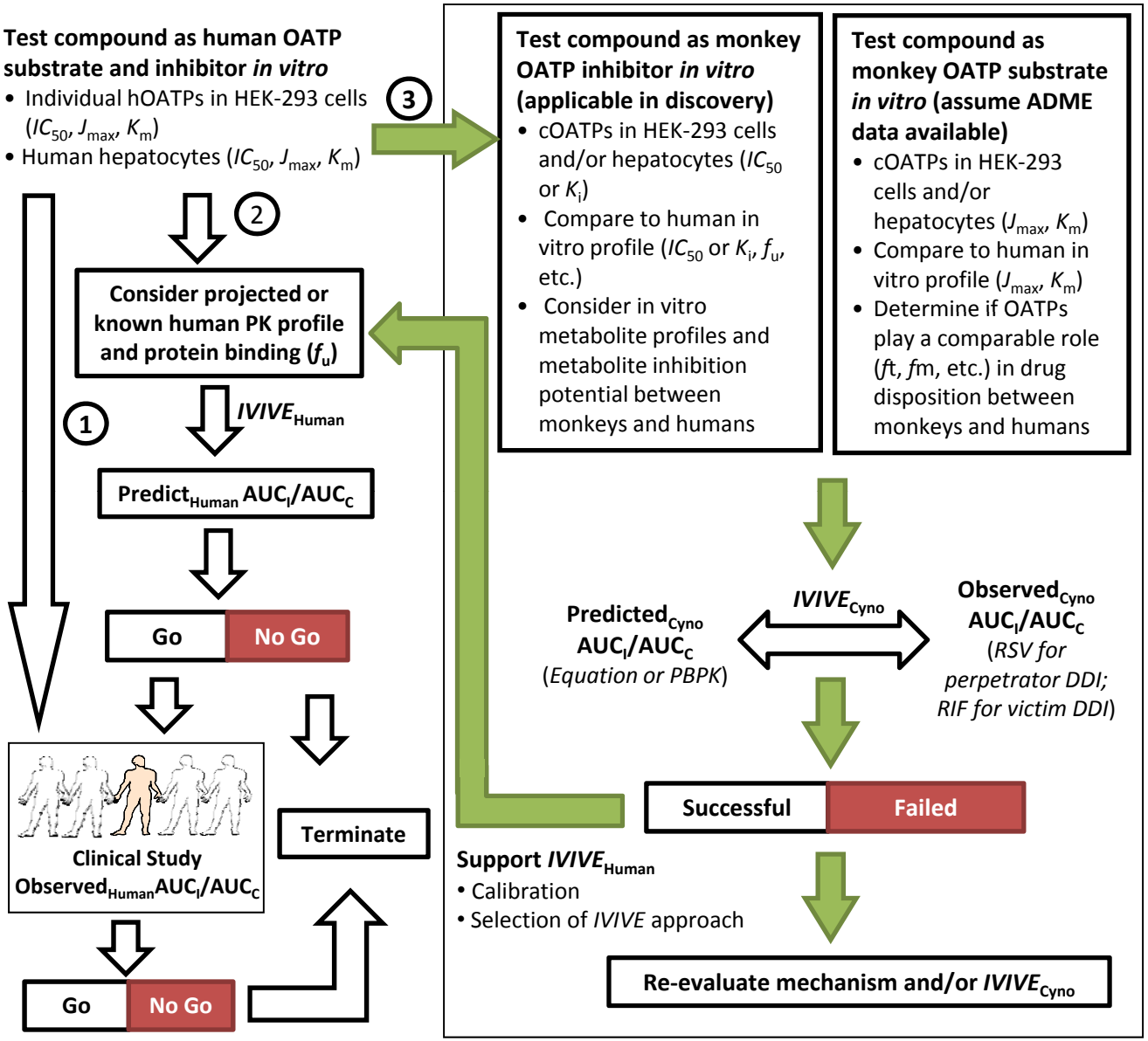

Figure 1

JPET Fast Forward. Published on January 7, 2013 as DOI: 10.1124/jpet.112.200691
This article has not been copyedited and formatted. The final version may differ from this version.

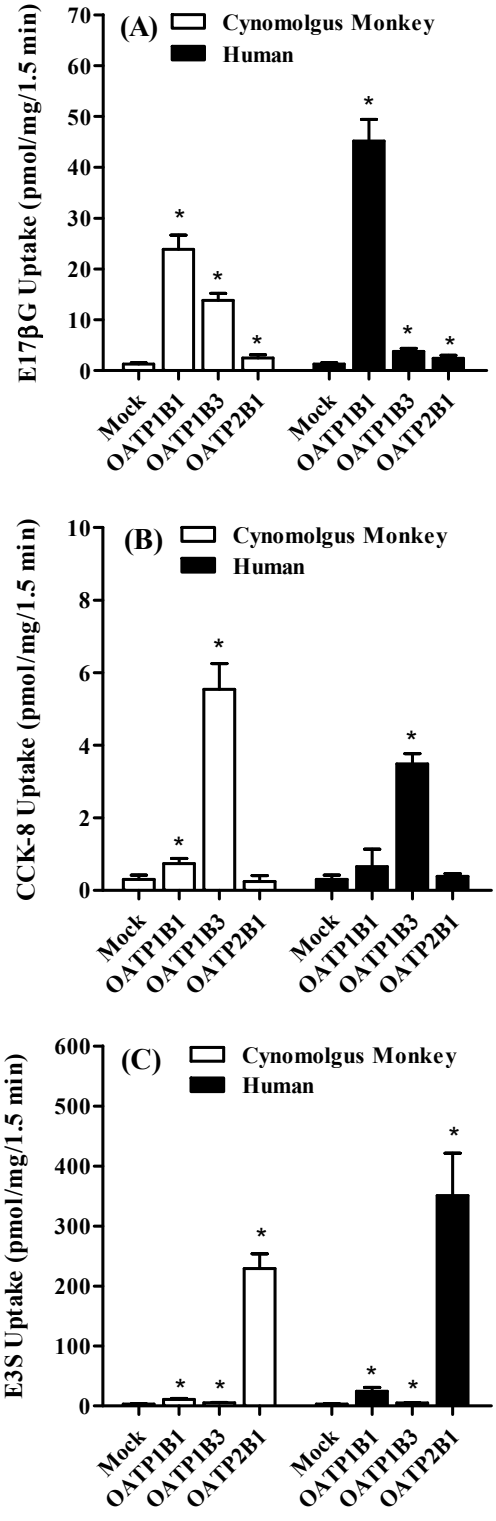

Figure 2

JPET Fast Forward. Published on January 7, 2013 as DOI: 10.1124/jpet.112.200691
This article has not been copyedited and formatted. The final version may differ from this version.

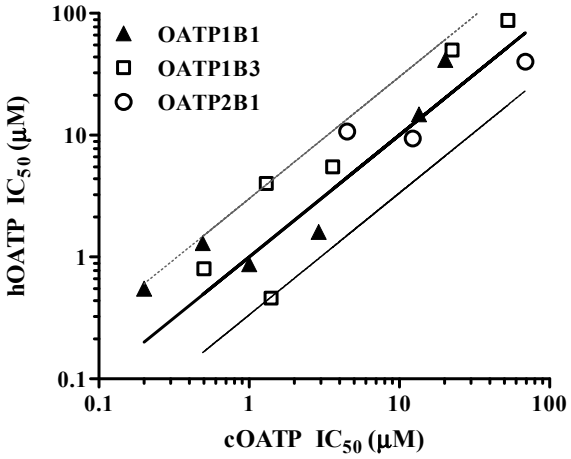

Figure 3

JPET Fast Forward. Published on January 7, 2013 as DOI: 10.1124/jpet.112.200691
This article has not been copyedited and formatted. The final version may differ from this version.

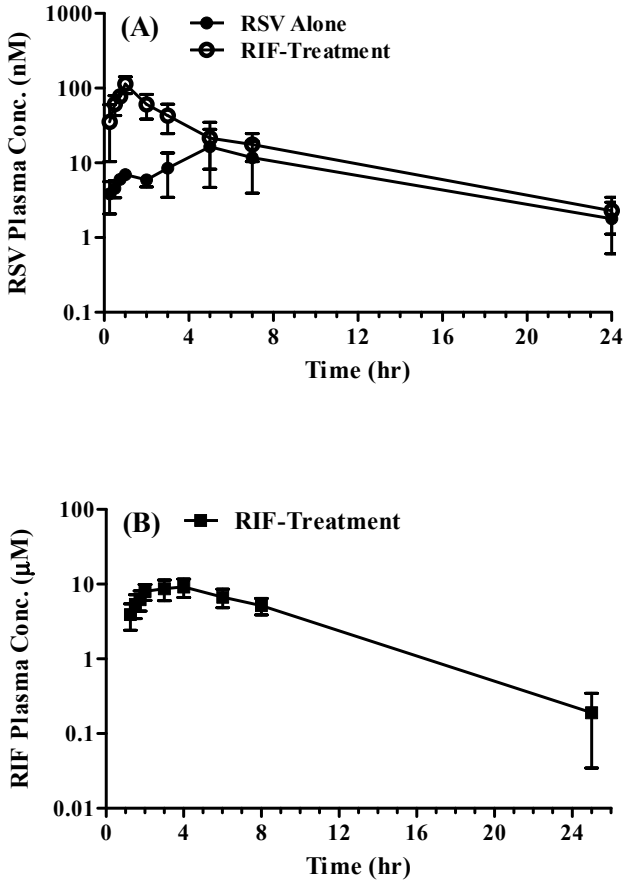

Figure 4

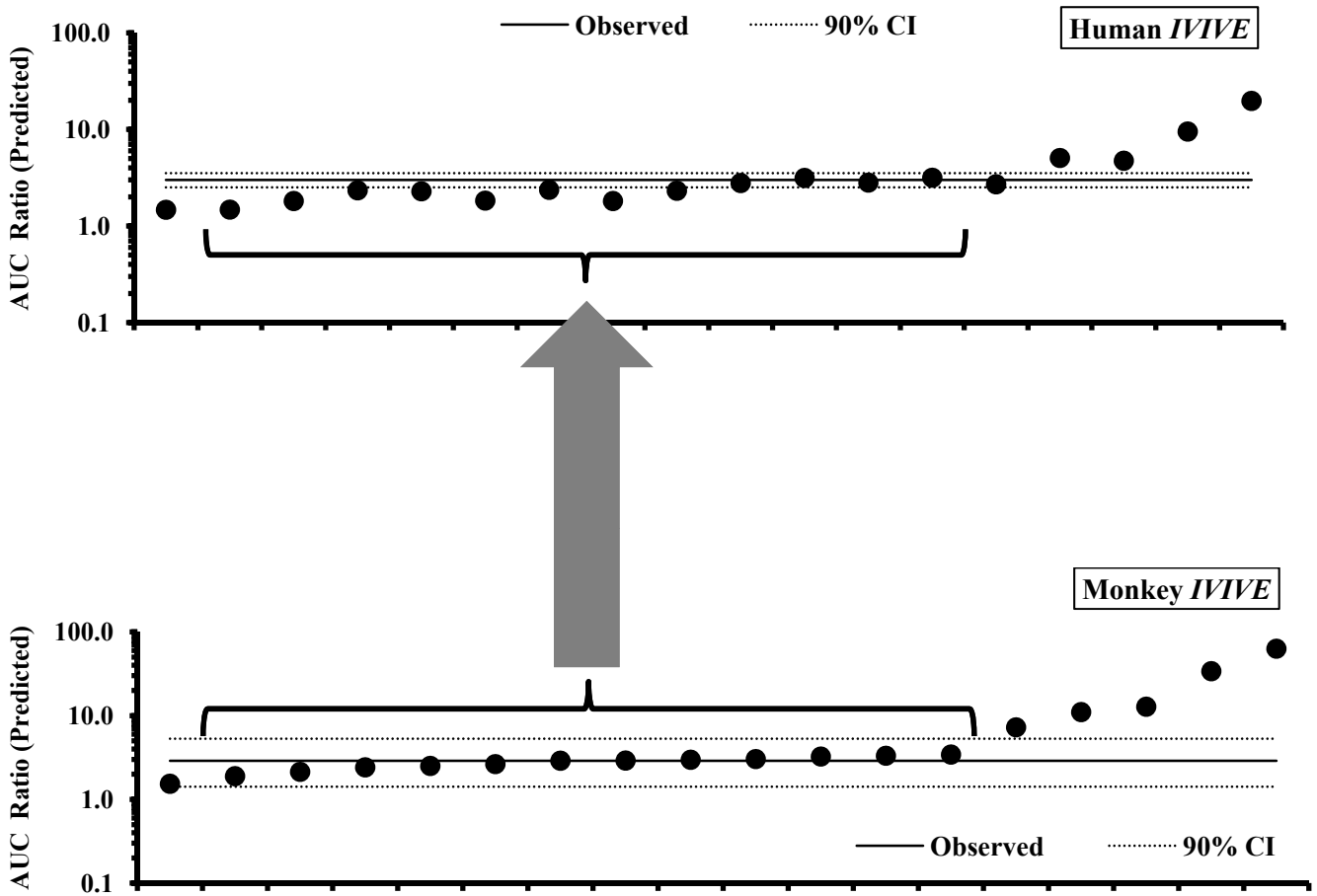

Equation	3	2	3	3	3	2	2	1	2	3	3	2	2	1	1	1	1	1
I_{max}			free			free				total		total		free			total	
I_{ave}	free	free		total			total	free							total			
$I_{in,max}$					free				free		total		total			free		total

Figure 5

Supplementary Figures

Cynomolgus Monkey As a Potential Model To Assess Drug Interactions Involving Hepatic Organic Anion Transporting Polypeptides (OATPs): In Vitro, In Vivo and In Vitro-In Vivo Extrapolation

Hong Shen, Zheng Yang, Gabe Mintier, Yong-Hae Han, Cliff Chen, Praveen Balimane, Mohammed Jemal, Weiping Zhao, Renjie Zhang, Sanjith Kallipatti, Sabariya Selvam, Sunil Sukrutharaj, Prasad Krishnamurthy, Punit Marathe, and A. David Rodrigues

Supplementary Figure 1
Alignment of the predicted amino acid sequences of cynomolgus (Cyno), rhesus (Rhes) and human (Huma) OATPs. The highlighted areas denote the difference between the sequences of cynomolgus, rhesus, or human for OATP1B1 (A), OATP1B3 (B) and OATP2B1 (C). cOATP1B1, cOATP1B3 and cOATP2B1 have been deposited in GenBank (Accession Nos. JX866725, JX866726 and JX866727, respectively).

Supplementary Figure 1A (OATP1B1)

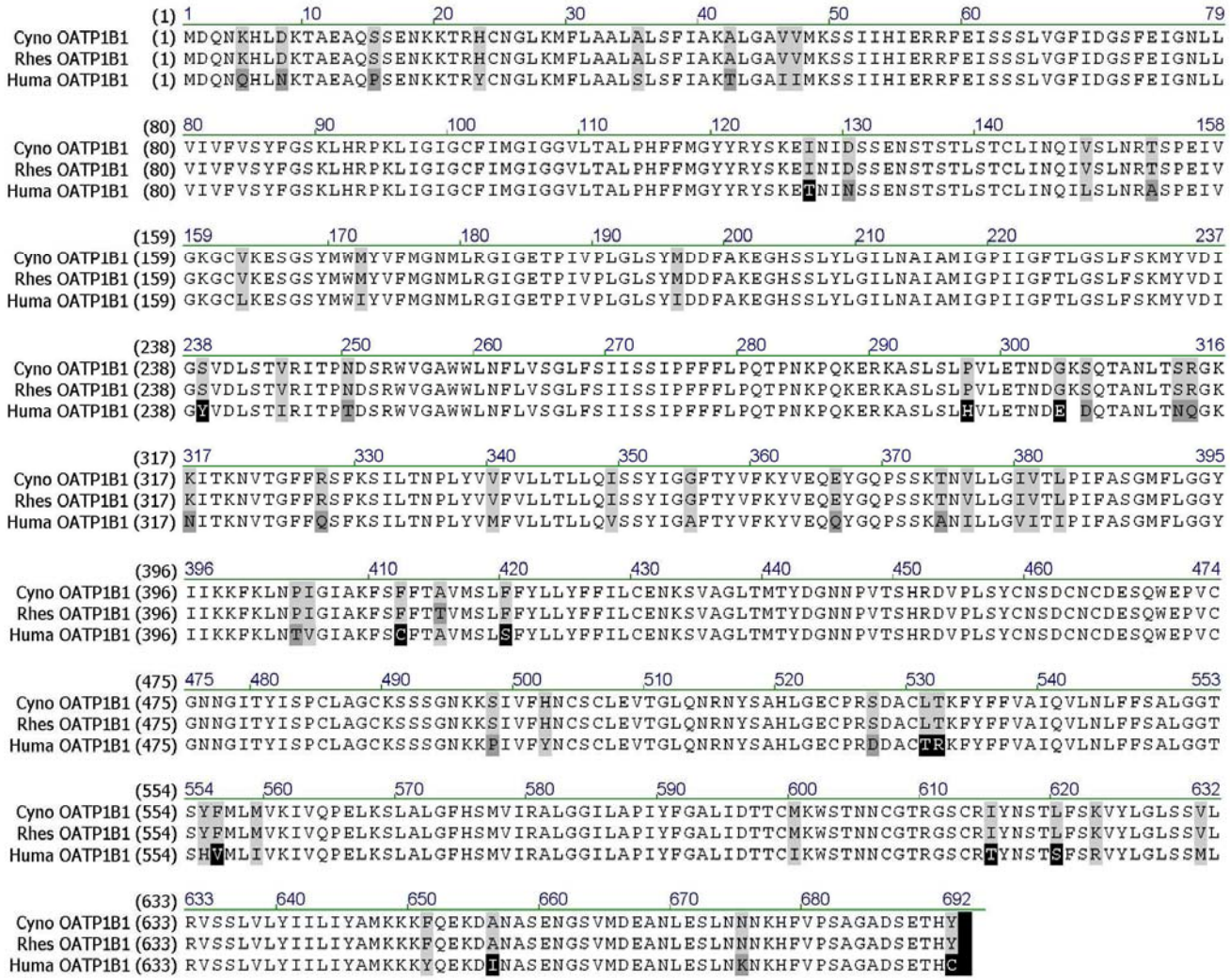

Supplementary Figure 1B (OATP1B3)

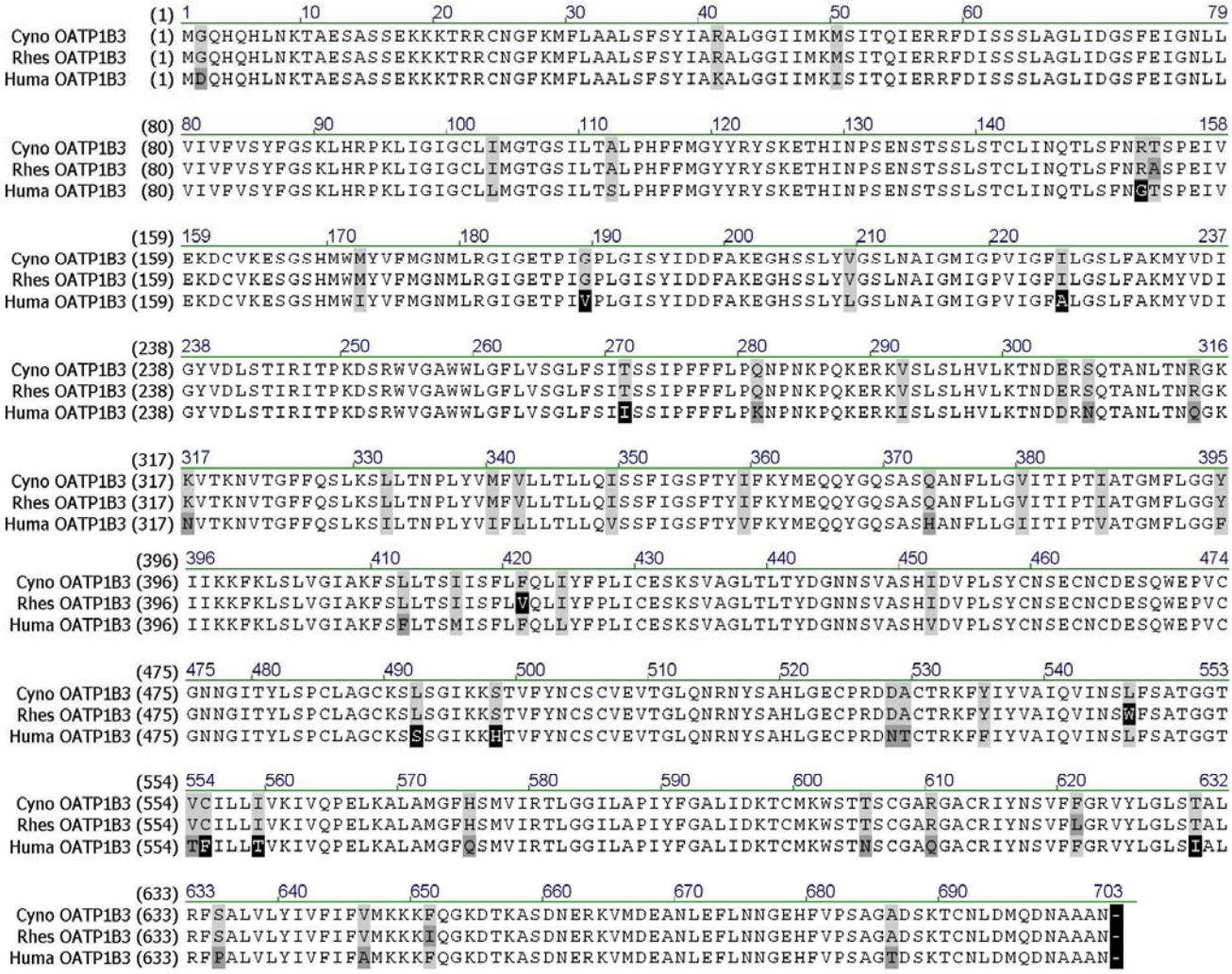

Supplementary Figure 1C (OATP2B1)

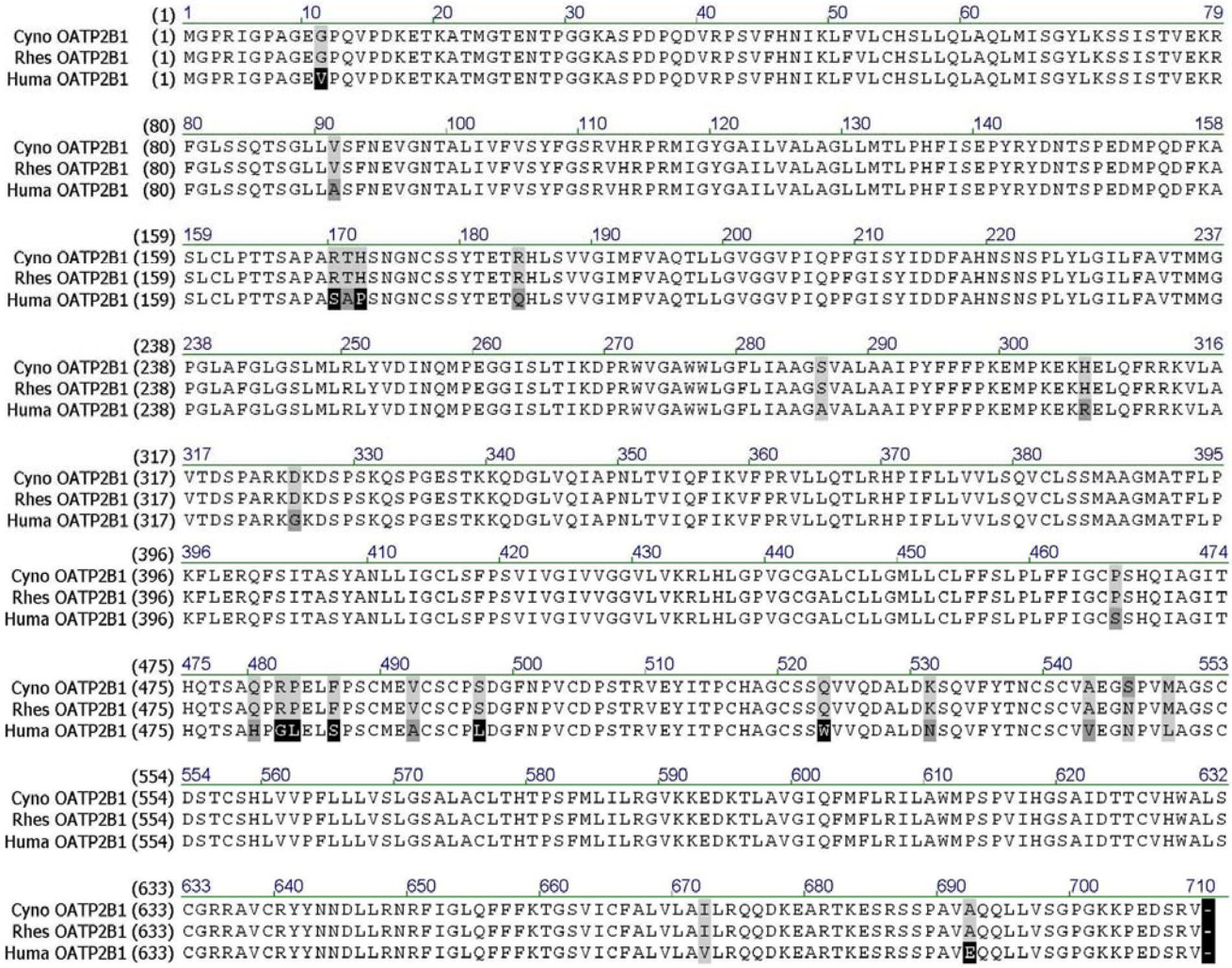

Supplementary Figure 2

Concentration dependent uptake rates (A and B), relative contribution of active and passive processes (C and D), and Eadie-Hofstee plots (E and F) of uptake [^{3}H]RSV by cynomolgus monkey and human hepatocytes. Symbols and the solid line represent observed values and the fitted curves to equation 5, respectively. Dashed and dotted lines represent active and passive uptake components, respectively.

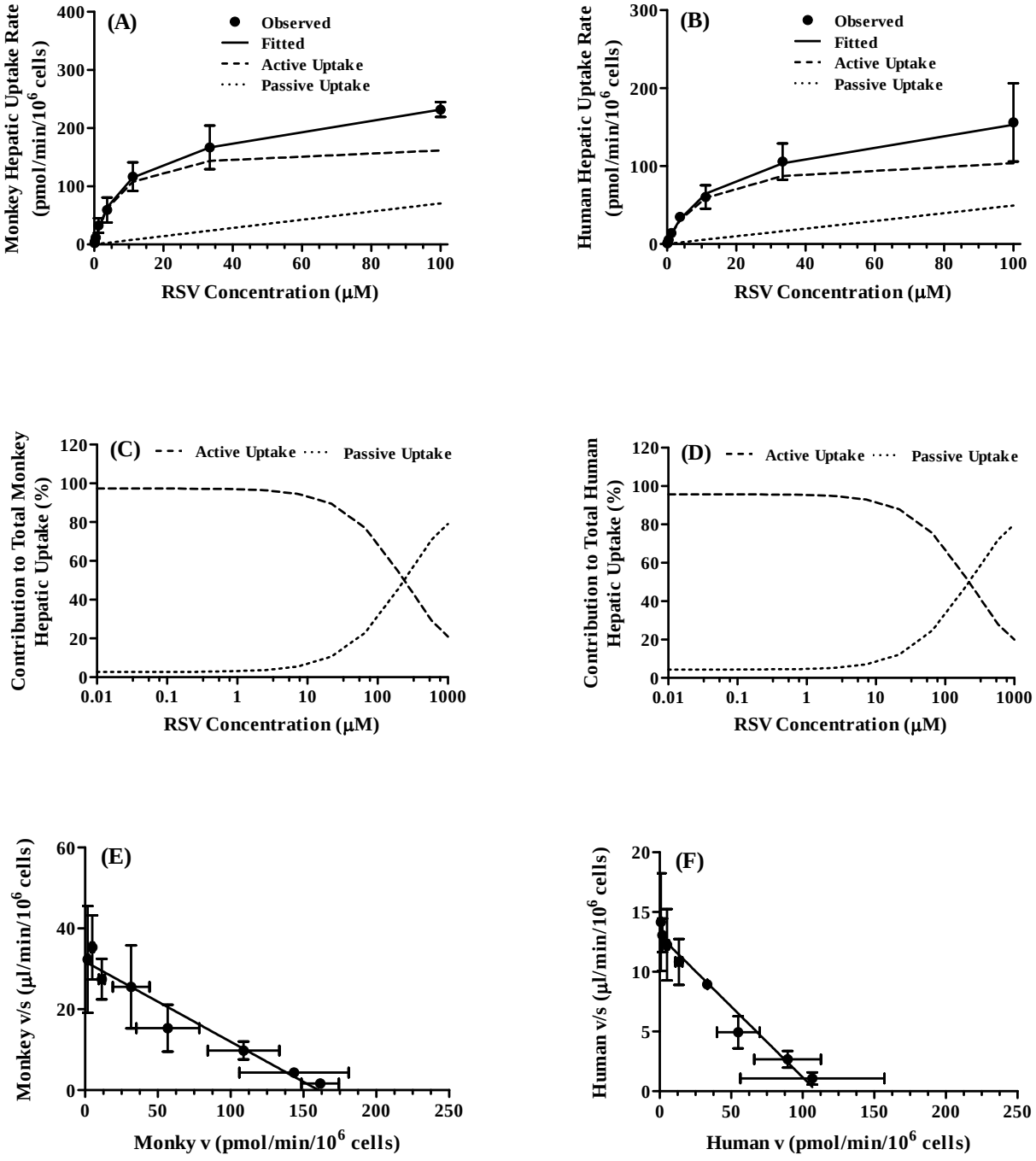

Supplementary Figure 3

Time course of uptake of [^{3}H]RSV (1 µM) by HEK 293 cells stably expressing cOATP (A) and hOATP (B). Uptake was performed by incubating cells with [^{3}H]RSV dissolved in HBSS buffer supplemented with 10 mM HEPES (pH 7.4) at 37 ˚C as described under *Materials and Methods* for different periods of time. Data are expressed as mean ± SD (n = 3 determinations)

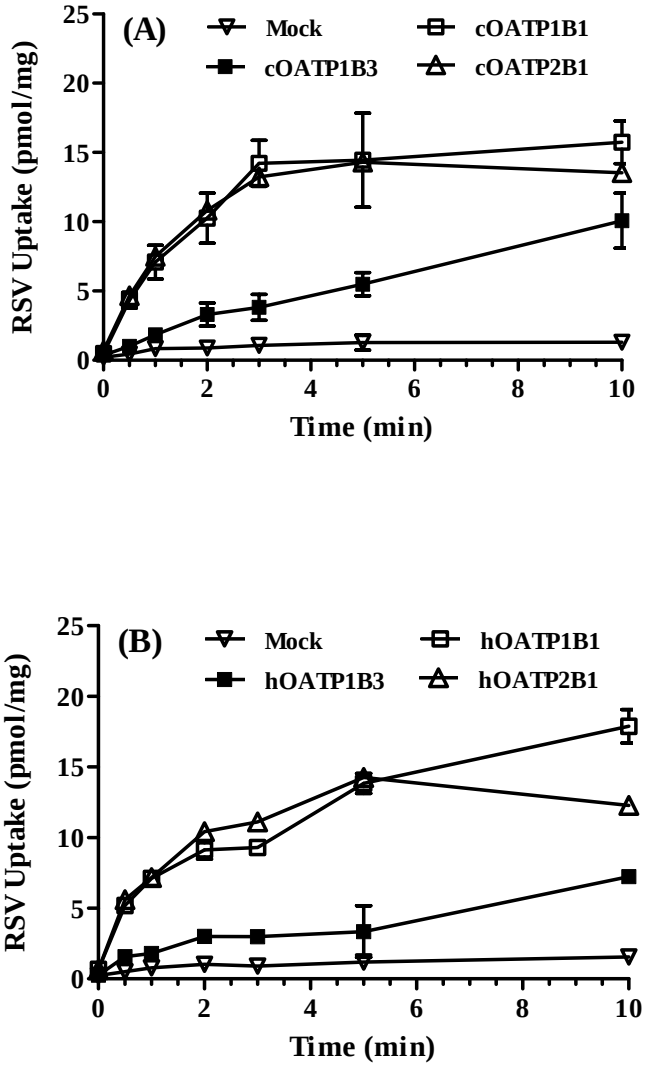

Supplementary Figure 4

Individual $AUC_{0\text{-}inf}$ (A), and C_{max} values (B) of RSV in 3 cynomolgus monkeys after a single oral dose of 3 mg/kg RSV with and without an oral RIF administration (15 mg/kg). The values of each individual are connected with a line.